Comparison of CO_2 Trapping in Highly Heterogeneous Reservoirs with Brooks-Corey and Van Genuchten Type Capillary Pressure Curves

Naum I. Gershenzon*[a], Robert W. Ritzi Jr. [a], David F. Dominic[a], Edward Mehnert[b], Roland T. Okwen[b]

[a]*Department of Earth and Environmental Sciences, Wright State University, 3640 Col. Glenn Hwy., Dayton, OH 45435, USA*

[b]*Illinois State Geological Survey, Prairie Research Institute, University of Illinois at Urbana-Champaign, 615 East Peabody Drive, Champaign, IL 6182, USA*

* corresponding author: naum.gershenzon@wright.edu

Abstract

Geological heterogeneities affect the dynamics of carbon dioxide (CO_2) plumes in subsurface environments in important ways. Previously, we showed how the dynamics of CO_2 plumes are influenced by the multiscaled sedimentary architecture in deep brine fluvial-type reservoirs. The results confirm that representing small-scale features and the corresponding heterogeneity in saturation functions, along with hysteresis in saturation functions, are all critical to understanding capillary trapping processes. Here, we show that when heterogeneity and hysteresis are represented, the two conventional approaches for defining saturation functions, Brooks-Corey and van Genuchten, represent fundamentally different physical systems. The Brooks-Corey approach represents heterogeneity in entry pressures, and leads to trapping by capillary pinning. The van Genuchten approach represents a network of pores transporting the nonwetting fluid, across rock types, with negligible capillary entry pressure, and leads to significant capillary retardation. These differences significantly affect the large-scale characteristics of CO_2 plumes (i.e., their mass, shape, and position).

Keywords: CO_2 geosequestration, capillary trapping, Brooks-Corey, van Genuchten, heterogeneity, sedimentary architecture

1. Introduction

The idea of reducing atmospheric carbon dioxide (CO_2) by capturing CO_2 from emission streams and injecting and permanently sequestering it the Earth's crust has been examined for decades (Gale et al. [14]). Multiple CO_2 sequestration research and demonstration projects have been operating worldwide since 1972. The critical question is whether injected CO_2 can be permanently stored in deep sedimentary basins without affecting groundwater quality? To answer this question detailed modeling of the migration and distribution of injected CO_2 in the subsurface is required.

Various processes may trap supercritical CO_2 (CO_2 hereafter) emplaced in deep brine reservoirs, including shorter-term physical trapping (0–10 years), intermediate-term dissolution

in brine (0–1,000 years), and longer-term mineralization (100 years–million years). Here, the focus is on the processes of physical trapping and dissolution taking place within the reservoir before a plume reaches caprock, and not on structural trapping by caprock at the top of the reservoir, or on mineralization.

A large body of experimental, theoretical, and numerical research now shows that capillary trapping has a primary impact on the distribution of CO_2 within the permeable sections of the reservoir, and field observations now confirm the formation and stability of capillary trapped CO_2 there, e.g., Krevor et al. [31]. There are two main capillary trapping processes:

(1) Carbon dioxide bubbles are trapped within pore spaces because of "snap-off" (Figure 1a), a process in which counter-imbibition of brine (the wetting fluid) behind the advancing plume, preferentially through smaller pores and pore throats, traps CO_2 bubbles within the intervening pore bodies (e.g., Hunt et al., [21]; Wildenschild et al., [58]; Iglauer et al., [24]). In conventional modeling approaches, this process is reflected in hysteresis in the constitutive relationship between relative permeability and phase saturation (e.g., Juanes et al., [26]; Spiteri et al., [53]; Joekar-Niasar et al., [25]). Snap-off trapping allows CO_2 to be distributed with a larger surface area, and thus enhances solution trapping. The process is lessened if the medium is not strongly water wet; however, in data reviewed by Iglauer et al. [23], most reservoir rocks exhibit water-wet behaviour, and the water-wet medium assumption is common in studies of capillary trapping. Altundas et al. [1] showed that hysteresis in the constitutive relationship between capillary pressure and saturation can also retard or halt the advance of the plume through the reservoir, because the pressure in the non-wetting phase at the leading edge of the plume must be sufficiently large for counter-imbibition to occur readily in the tail region. The effect of this process was shown to be small relative to snap-off trapping under the conditions they explored.

(2) Capillary trapping can be caused by heterogeneity in the capillary entry pressure among reservoir rock types [5, 10, 15, 16, 51, 60]. In this process (Figure 1b), CO_2 is pinned below local contacts between an underlying reservoir rock type with larger pores and an overlying reservoir rock type with smaller pores and thus larger entry pressure. This pinning can occur even within the permeable sections of the reservoir where the entry pressure of smaller scale, relatively finer-grained textural units (e.g. finer-grained sandstone) exceeds the buoyant pressure of the CO_2 in the underlying coarser-grained textural units (Figure 1b). During injection, CO_2 preferentially enters the higher-permeability, coarser-grained regions. As discussed by Meckel et al. [46], flow

behaviour at a distance away from the injection well and behaviour everywhere after injection ends is dominated by buoyant and capillary forces (viscous forces are negligible) and controlled by their differences across such contacts. As with snap-off trapping, capillary pinning increases the surface area of the CO_2 phase and thus enhances solution trapping. Gershenzon et al. [15, 16] investigated the relative effect of these physical trapping processes in a cross-bedded fluvial reservoir containing both coarser- and finer-grained cross-beds, as discussed below. As we show below, the capillary pinning could be permanent (Figure 1b) or transient (Figure 1c).

In the following, we will use three terms to designate capillary trapping: "snap-off", "capillary pinning," and "capillary retardation". The latter term is for the transient capillary pinning.

Figure 1.

The conventional approach for modeling of CO_2 plume dynamics uses functions or tables to represent the relationships of capillary pressure and relative permeability with saturation. The shape and particular parameters of these curves, such as irreducible water saturation, S_{wi}, maximum residual gas saturation (saturation trapped by snap-off), S_{gr}, and the entry pressure, P_e, play a key role in the trapping processes and define the rate and amount of trapped CO_2, as well as the shape and dynamics of the CO_2 plume [1, 7, 10, 14, 26, 28, 32, 39, 47, 53]. Two models commonly used to represent the capillary pressure saturation curves are the Brooks-Corey [4] and the van Genuchten [56] models. Hereafter, we will use the abbreviations BC and vG to designate Brooks-Corey and van-Genuchten, respectively.

The main difference between the vG and BC models is that the BC model represents an entry pressure (capillary pressure is not equal to zero at water saturation equal to zero) and the vG model does not. The vG model represents the existence of at least one connected pore-pathway with pores large enough so that the capillary pressure is negligible. Capillary pinning in these two cases are different. Let us first describe the capillary pinning effect in the BC case. Consider a FG textural unit underlain by a CG unit (Figure 2). If for a given CO_2 saturation, S_{CG}^w, capillary pressure in the CG unit, $P_c(S_{CG}^w)$, is less than the entry pressure in overlain FG unit, $P_c(S_{FG}^w = 1) \equiv \mathrm{P}_{e,FG}$, minus the buoyant force per unit area, i.e. if $P_c(S_{CG}^w) < \mathrm{P}_{e,FG} - (\rho_w - \rho_{CO2})gh$ (here g is gravitational acceleration and h is the height of the CO_2 layer), then CO_2 from the CG unit will be unable to penetrate to FG unit (Figure 2a). In this case CO_2 is trapped in the

underlying CG layer. In vG case (Figure 2b) as long as the brine saturation in the FG unit exceeds S_{FG}^{w}, some amount of buoyant CO_2 (as a non-wetting fluid) may freely penetrate the overlying rock without any capillary pressure barrier. However, because CO_2 will not enter the overlying unit when *Pc* in the overlying exceeds $P_c(S_{CG}^{w})$, capillary pressure will limit the rate at which CO_2 saturation can increase in the overlying unit, and give rise to a process we refer to below as 'capillary retardation'. As we show, capillary retardation can cause a significant delay in the rise of the plume, and promote dissolution trapping. Importantly, we show that the differences between BC and vG saturation functions, one leading to capillary pinning, the other to capillary retardation, can considerably change the amount of trapped and dissolved CO_2 as well as the dynamics and shape of CO_2 plumes in heterogeneous reservoirs.

Figure 2

Li et al. [39] investigated the difference between simulations of CO_2 sequestration in homogeneous aquifers using these two models. They observed that (1) the vG capillary pressure model accelerates CO_2 solubility trapping compared with the BC model; and (2) simulation results are very sensitive to the slope of the vG curve in the vicinity of maximum brine saturation.

Geological heterogeneities fundamentally affect the dynamics of a CO_2 plume in subsurface environments [2, 5, 12, 18, 20, 22, 29, 40, 47, 49, 51, 54, 60]. Bryant et al. [5] and Ide et al. [22] showed that a layer of smaller permeability lying above a layer of larger permeability can cause a pinning effect. Saadatpoor et al. [51] further illustrated this trapping mechanism by assuming a functional dependence between permeability and capillary pressure, and simulating the dynamics of the buoyant CO_2-brine front in a heterogeneous reservoir. Comparison of this simulation with an analogous simulation, but with a homogeneous (averaged) capillary pressure curve, revealed a dramatic difference in results. In the former case, CO_2 rises through the high-permeability channels, which are surrounded by the capillary barriers of the low-permeability material. In some regions capillary barriers prevent upward movement of CO_2, allowing only lateral migration, which effectively traps the CO_2 plume. The same idea was explored by Zhou et al [60]. Considering regional-scale flow and transport processes in a layered reservoir, CO_2 accumulated between layers with different permeability and capillary-pressure entry points, causing retardation of upward CO_2 migration. Krevor et al. [29] and Pini et al. [49] provided laboratory evidence showing that sub-core scale heterogeneity can control CO_2 saturation. They

demonstrated that CO_2 plumes can be immobilized behind capillary barriers as a continuous phase [29]. The variability of the capillary pressure-saturation curves measured in the laboratory is caused by the presence of millimeter-scale heterogeneities in a sample [49]. Li and Benson [40] further investigated how millimeter-scale heterogeneities affect large-scale CO_2 migration by the local capillary barriers. In particular, they showed that these heterogeneities may significantly reduce (by a factor of two) the CO_2 frontal speed during buoyancy-driven migration. Trevisan et al. [54] experimentally studied the influence of larger-size heterogeneity (centimeter–meter) that contributes to the distribution of a CO_2 plume in a brine-saturated reservoir. They found that (1) spatial variability of capillary entry pressure controls plume dynamics in capillary-dominated flow regimes; and (2) heterogeneity influences plume spreading mainly during the short-term injection period, while long-term trapping performance of heterogeneous models can be reproduced by Land's models fitted to homogeneous models with analogous mean permeability.

Some potential CO_2 reservoirs have sedimentary architecture reflecting fluvial deposition (Figure 3). Gershenzon et al. [15, 16] investigated how such fluvial architecture can affect the dynamics of a CO_2 plume during and after injection. They used new three-dimensional geocellular models representing the field-observed spatial arrangement of coarser-grained (CG) cross-bed sets (24% volume fraction in their study) juxtaposed with finer-grained (FG) cross-sets (76%). These models also represent how these cross-sets are organized within a hierarchy of larger-scale features [42, 43]. Heterogeneity in the constitutive relationship models was represented by using separate BC models for each cross-set type. Given the contrast in entry pressures, capillary pinning was pronounced and all CO_2 was effectively immobilized by the combination of snap-off trapping, capillary pinning, and dissolution, before reaching the top of the reservoir.

Here, we expand on the work by Gershenzon et al. [15, 16] and Li et al. [39] by including vG models as well as BC models to represent the capillary pressure saturation function, as it varies with rock type in a reservoir with fluvial architecture. We show that capillary and dissolution trapping are very different for the BC and vG approaches under the type of reservoir heterogeneity represented here.

Figure 3.

2. Methodology

Many existing and potential CO_2 reservoirs have fluvial sedimentary architecture, e.g., Mt. Simon Sandstone [13], the lower Parratte Formation [6, 30], the Victor interval of the Ivishak Formation [55], and the lower Tuscaloosa Formation [30, 41]. The heterogeneity in permeability of these reservoirs is defined by their fluvial architecture ranging from the centimeter to the reservoir scale. The sedimentary architecture of some of these reservoirs has been quantified in three-dimensional models [3, 17, 42, 44, 50]. To create a geocellular model of fluvial reservoir architecture, we use the methodology described in Ramanathan et al. [50]. We generated a realization of the channel-belt architecture, including two textural facies: FG rocks (76%) and CG rocks (24%). The proportion of CG rocks affects the proportion of high-permeability cells that are connected to create preferential flow pathways. In the realization we created, 71% of CG cells are connected in one spanning cluster. This model has been used to create a map of intrinsic permeability suitable for simulation of CO_2 distribution in fluvial reservoirs (Figure 4). The geometric mean of permeabilities is as follows: 58 mD among FG cells, 3823 mD among CG cells, and 193 mD among all cells.

Figure 4.

The reservoir size is 100 m × 100 m × 5 m (250 thousand cells of size 2 m × 2 m × 0.05 m). The CO_2 was injected at a rate of 0.03025 kg/s for 10 days into the bottom of a vertical well at a depth of 2360 m. Our simulations covered a total of 1,010 days or 1,000 days post-injection. The pressure and temperature at the top of the reservoir are 230.8 bar and 53°C, respectively, such that the injected CO_2 was supercritical. The well was placed at x = 23 m and y = 1 m. No-flow boundaries were imposed on all boundaries of the CO_2 reservoir. The total amount of injected CO_2 is 26136 kg. For the simulations, both the heterogeneous reservoir described above (Figure 4) and a homogeneous reservoir with intrinsic isotropic permeability of 193 mD (equal to the geometric mean of the permeability of the heterogeneous reservoir) were used.

Two different sets of characteristic curves were utilized for the FG and the CG rock types. Thus, the total number of characteristic curves was 12 (Figure 5), including six for drainage and six for imbibition. To generate the curves, we used the following methodology that adapted the approach of Holtz [19]. First, using an empirical relation between permeability (k) and porosity ($\emptyset$), we obtained porosity for FG and CG rocks (Table 1, column 2):

$k = 7 \cdot 10^7 \emptyset^{9.61}$ in mD. (1)

Then, we found the averaged irreducible water saturation (S_{wi}) and residual CO_2 saturation (S_{gr}) for both facies types by formulae (Table 1, columns 4 and 5):

$S_{wi} = 5.159(\log(k)/\emptyset)^{-1.559}$; (2)

$S_{gr} = -0.969\emptyset + 0.5473$. (3)

The next step was to calculate capillary pressure for drainage (P_{cd}) using the Brooks-Corey relation [4]:

$P_c = P_e(\frac{S-S_{wi}}{1-S_{wi}})^{-1/\lambda}$, (4)

where S is water saturation, P_e is the minimum pressure required for the entry of CO_2 into the pore of the rock, and λ is a fitting parameter known as pore-size distribution index. For rocks from the Mt. Simon Sandstone, $P_e = 0.046$ bar and $\lambda = 0.55$ [30]. We used this value for the FG rocks. To find the entry pressure point for the CG rocks, we scaled the FG rocks value based on the Leverett *J*-function as proposed by Saadatpoor et al [51]:

$P_e^{CG} = P_e^{FG}(\frac{k_{FG}\phi_{CG}}{k_{CG}\phi_{FG}})^{0.5}$. (5)

For imbibition, we used a curve analogous to (4) but, in contrast to drainage, the imbibition curve crosses the saturation axis at a value of $S = 1 - S_{gr}$.

For the relative permeability curves, the Brooks-Corey relations in the form proposed by Dullien [8] were used:

$k_{r,w} = (S_w^*)^{N_w}$; (6)

$k_{r,CO2} = k_{r,CO2}(\mathrm{S}_{wi})(1-\mathrm{S}_w^{**})^2[1-(\mathrm{S}_w^{**})^{N_{CO2}}]$, (7)

where $S_w^* = \frac{S-S_{wi}}{1-S_{wi}}$, $S_w^{**} = \frac{S-S_{wi}}{1-S_{gr}-S_{wi}}$. The variables N_w and N_{CO2} are fitting parameters known as the Corey exponents for water and CO_2, respectively. The following values were used: $N_{CO2} = 4$ [30] and N_w = 5 and N_w = 3 for drainage and imbibition, respectively.

The values of other parameters are in Table 1. The results are summarized in Figure 5.

Table 1. Data for relative permeability and capillary pressure curves for the BC case. The values of S_{wi}, S_{gr}, $k_{r,CO2}(\mathrm{S}_{wi})$, and P_s^{OFC} are calculated by formulae (1–7). The values of P_s^{SS} and ∅ are from [30].

	∅	λ	S_{wi}	S_{gr}	$k_{r,CO2}(S_{wi})$	P_e (bar)
FG rocks	0.23	0.55	0.22	0.32	0.65	$4.6 \cdot 10^{-2}$
CG rocks	0.36	0.55	0.14	0.20	0.95	$0.72 \cdot 10^{-2}$

To generate a vG-type capillary pressure curve we followed Li et al. [39] and used the same relation (4) in the range $S_{wi} \le S \le (1 - S_{nt})$ and the relation (8) if $1 - S_{nt} < S \le 1$ (Figure 6):

$$P_c = (1 - S)\frac{P_e}{S_{nt}}\left(\frac{S - S_{nt} - S_{wi}}{1 - S_{wi}}\right)^{-1/\lambda} . \quad (8)$$

There is no difference between the BC and vG types for imbibition curves.

Figure 5.

Figure 6.

We also created a "true" vG curve using the conventional formula:

$$P_c = P_g[(S_w^*)^{-1/m_g} - 1]^{1/n_g},\ m_g = 1 - 1/n_g, \quad (9)$$

where P_g is a pressure scaling parameter related to the average size of the pores. The exponents m_g and n_g are related to the pore-size distribution. The values of these parameters were chosen based on the BC parameters in the formulas proposed by Lenhard et al. [34]. Thus, we used the following values: $P_g(\mathrm{CG}) = 1.13 \cdot 10^{-2}$ bar, $P_g(\mathrm{FG}) = 7.24 \cdot 10^{-2}$ bar, and $n_g = 1.668$.

ECLIPSE-300 (compositional model with the CO2STORE option) has been used for simulations. Four components were included in simulations: H_2O, CO_2, NaCl, and $CaCl_2$ with initial total phase mole fractions of 0.9109, 0, 0.0741, and 0.015, respectively. The water compressibility and viscosity are $4.35 \cdot 10^{-5}$ 1/bar and 0.813 cP, respectively. Killough's hysteresis model for history-dependent capillary pressure and relative permeability functions [27] has been used, i.e., snap-off saturation of CO_2, relative permeability, and capillary pressure were calculated based on the formulae (34.1–4) and (34.20–21) described in the ECLIPSE manual [45]. The mutual solubilities of CO_2 and H_2O were calculated following the procedure given by Spycher and Pruess [52]. The gas density was obtained by a tuned cubic equation-of-state. The CO_2 viscosity was calculated based on the procedure described by Fenghour et al. [11] and Vesovic et al. [58].

3. Results

The results for the homogeneous simulations are discussed first. In both (with BC and vG curves) homogeneous simulations, the plumes reached the top of the reservoir and spread under the impermeable boundary. Figure 7 shows the plume shape after 1,010 days. The dynamics of CO_2 trapping by snap-off through the simulation are shown in Figure 8. The trapping by snap-off is the same in both homogeneous simulations because the same relative permeability saturation functions were used. The majority of the CO_2 (75.7%) is trapped by snap-off at the end of the simulation. The dynamics of trapping by dissolution are shown in Figure 9, and the dynamics of CO_2, eventually trapped by the impermeable top, are shown in Figure 10. Table 2 summarizes the distribution of CO_2 at the end of the simulation. The difference between the homogeneous simulations is that the simulation using the vG model has more trapping by dissolution compared to the simulation using the BC model, as seen clearly in Table 2, and thus less CO_2 reaches the top. This is the main reason why the plume in the BC case is wider (Figure 7). These results are consistent with Li et al. [39].

Figure 7.

Figure 8.

Figure 9.

Figure 10.

Table 2. Mass distribution of CO_2 (fraction from the total amount of injected CO_2) at the end of the simulation.

	Trapped by snap-off			**Trapped by pinning**	**Trapped by dissolution**			**Mobile**
Homogeneous BC	0.754			0	0.158			0.088 (trapped by seal)
Homogeneous vG	0.757			0	0.193			0.050 (trapped by seal)
	CG	**FG**	**Total**		**CG**	**FG**	**Total**	
Heterogeneous BC	0.362	0.215	0.577	0.159	0.067	0.197	0.265	0
Heterogeneous	0.290	0.352	0.642	0.003	0.076	0.303	0.355	0

vG1								
Heterogeneous vG2	0.303	0.303	0.606	0.005	0.083	0.306	0.389	0

In the heterogeneous simulations, the plumes do not reach the top of the reservoir at the end of the simulations (Figure 11). Importantly, the reason the plumes do not reach the top is very different between simulations using the BC and vG models. With the BC model, the CO_2 that is not trapped by snap-off or dissolution is immobilized by capillary pinning. With the vG model, all the CO_2 is trapped by snap-off and dissolution and there is essentially no mobile CO_2. A study of Figures 8–12 and Table 2 brings out these and other subtle differences.

Figure 11.

Figure 12.

With either model, CO_2 preferentially enters the more permeable CG cells during injection. With the vG model, the CO_2 more readily crosses into FG cells; the plume spreads into more of the reservoir, and thus more (by 12%) snap-off trapping occurs (Figure 8). Indeed, Figure 12 and Table 2 show that more snap-off trapping occurs in FG rocks with the vG model than in CG rocks, because the plume occupies more pores space in FG rocks. The opposite is true with the BC model. Note that ECLIPSE has the ability to calculate snap-off trapping and the amount of mobile CO_2, which includes capillary-pinned CO_2. In cases where CO_2 did not reach the top of the reservoir, the total amount of so-called mobile CO_2 is capillary pinned.

With the BC approach, CO_2 is trapped within connected clusters of CG cells that do not span the domain, and the CO_2 remains immobile unless the buoyancy force is sufficient to overcome the capillary entry pressure of FG rocks, as discussed in Gershenzon et al. [15]. In spanning clusters, CO_2 propagates mainly in the horizontal direction because the lengths of lateral branches of spanning CG clusters are greater than their local thickness. This happens initially during injection when viscous forces exceed buoyancy forces, and at all times when buoyancy forces are smaller than capillary forces. In the latter case, a lateral pressure gradient forces CO_2 to move along a boundary between CG rocks (lower capillary entry pressure) and the overlying FG rocks (higher capillary entry pressure). Also, the downward dip of CG cross-sets has a significant influence, creating a local downward component to velocity vectors inside a CG cross-set, and giving rise to local trapping within them during the post-injection phase. The CO_2 can exit from a spanning and downward dipping CG cluster across its upper boundary if the

297 buoyancy force is large enough. It will propagate upward into and through an overlying FG
298 cross-set and into the next CG cross-set above, responding to both buoyancy and capillary forces.
299 This process continues until the buoyancy force becomes comparable to the capillary force, and
300 then the plume becomes immobile or trapped without reaching the top of the reservoir.

301 The amount of dissolution trapping between heterogeneous simulations using the vG and BC
302 models is seen in Figure 9 and Table 2. As with the homogenous simulations, there is more
303 dissolution trapping when the vG model is used because, without capillary pinning, the CO_2
304 more readily crosses into FG cells and is distributed with a larger surface area, promoting
305 dissolution. By the end of the simulation, 35.5% of the CO_2 (Table 2) is trapped in the vG
306 simulation and only 26.5% in the BC simulation.

307 The most significant result is that at the end of the simulation time, the simulation with the
308 BC model still has a significant amount of CO_2 essentially immobilized by entry-pressure
309 pinning within CG cross-sets (15.9% of the source), whereas almost all of the CO_2 was trapped
310 by snap-off or dissolution in the simulation with the vG model. All CO_2 is trapped in either case,
311 yet the distribution of CO_2 is quite different (Figure 11).

312 To study the influence of the size of S_{nt} (the "tail" within the vG capillary curves), another
313 heterogeneous simulation was run with S_{nt} = 0.04, i.e., 2.5 times smaller than in the previous
314 simulation. Results were then compared for the BC, vG1 (S_{nt} = 0.1), and vG2 (S_{nt} = 0.04)
315 approaches. Table 2 shows that (1) the amount of mobile CO_2 in the gas phase for vG2 is a little
316 bit larger than for vG1 but still much smaller than for BC; (2) the amount of trapped CO_2 in the
317 gas phase for vG2 is smaller than for vG1 but still larger than for BC; and (3) the amount of
318 dissolved CO_2 for vG2 is a little bit larger than for vG1 and much larger than for BC. Thus, in
319 the range considered, the value of S_{nt} does not significantly affect the results.

320 We also created a simulation with the vG model calculated by equation (9). Comparison with
321 results using the vG model from Figure 6 (calculated by equations (4) and (8)) shows negligible
322 differences in the amount of trapped and solute CO_2 between these two cases. This indicates that,
323 as we expected, the main difference in results by using BC vs. vG capillary pressure curves is
324 due to the lack of an entry pressure in the vG case, and that the size of the vG tail or particular
325 equation used for the vG model are less important.

326 Regardless of the shape of the capillary pressure curves, the lack of entry pressure in the vG
327 model suggests that all mobile CO_2 (not trapped by snap-off and not dissolved) will eventually

migrate to the caprock. This is not the case in the BC approach; mobile CO_2 trapped by the capillary pinning will never reach the caprock. To illustrate this fundamental difference, we ran heterogeneous simulations with the same conditions as above but with no snap-off trapping (that is, with the value of maximum residual gas saturation equal to zero and hysteresis turned off) and for a longer period of time (10,000 days). The results are shown in Figure 13. With the vG model, almost all mobile CO_2 accumulates at the top of reservoir, but, with the BC model, CO_2 is trapped by capillary pinning.

Figure 13.

The simulations with heterogeneity better reflect geologic reality for fluvial sandstones. Note that fluvial architecture causes CO_2 to propagate predominantly in the lateral direction, creating strong effective permeability anisotropy. A comparison of the homogeneous simulations to the more realistic heterogeneous simulations shows the importance of representing heterogeneity in the constitutive relationships, regardless of whether or not an entry pressure exists. The homogeneous simulations overestimate the amount of snap-off trapping, underestimate the amount of solution trapping, and underestimate the total amount of trapping within the reservoir regardless of the approach for specifying capillary pressure curves.

To examine the sensitivity of the simulations to grid spacing, we compare the results of calculations with "normal" grid size, $2 \times 2 \times 0.05$ m, and with a grid size 8 times smaller, $1 \times 1 \times 0.025$ m. To make the computation feasible with a finer grid (number of cells is 160K), we use a small part of the original heterogeneous reservoir for simulation (number of cells $20 \times 20 \times 50 =$ 20K). We found that (1) positions and shapes of the plumes are virtually the same; (2) the difference in reservoir pressure is negligible; (3) the difference in amount of snap-off trapping is about 2% for both BC and vG cases; (4) the difference in amount of dissolution is up to 10% , (about 3% from the total CO2 amount). This allows us to conclude that the results were not sensitive to the grid resolution used.

4. Discussion and Conclusions

Simulation of CO_2 sequestration requires knowledge of capillary pressure–CO_2 saturation relations. These functional dependences are difficult to derive experimentally and are quite uncertain for most potential reservoirs. Conventionally, these curves are derived from experiments on a few samples and modeled using the Brooks and Corey [4] or van Genuchten

[56] approaches. The main difference between these two approaches is in the form of the capillary pressure curve where CO_2 saturation is small. Our results show that the presence or absence of an entry pressure in the capillary pressure curve at low CO_2 saturation significantly affects the rate and amount of CO_2 trapping. Therefore, distinguishing the true capillary pressure at small CO_2 saturation may be important.

Li et al. [39] found that CO_2 dissolution was affected by the shape of the capillary pressure tail in homogeneous reservoirs, but capillary trapping (snap-off) was insensitive to this shape. Here, we investigated the difference in CO_2 trapping (both dissolution and capillary trapping) between the BC and vG approaches to define capillary pressure curves for a heterogeneous reservoir, including two types of cross-strata (FG and CG). We found:

1. Carbon dioxide capillary trapping is significantly impacted by the type of capillary pressure curve used. Snap-off trapping averaged over the whole reservoir is somewhat larger for the vG approach. However, the larger difference is the amount of CO_2 trapped by capillary pinning, in the BC approach vs. the capillary retardation in the vG approach. As a result, mobile CO_2 eventually reaches the caprock in the vG approach, but never reaches the caprock with the BC approach. Also, note that a larger amount of CO_2 is trapped in CG rocks relative to FG rocks with the BC approach, whereas the opposite is true with vG approach. Thus, the distribution of CO_2 is quite different between the two approaches.

2. Heterogeneity increases the surface area of the plume and therefore dissolution trapping is enhanced. This is a logical extension of the results by Li et al. [39], who showed that changes to the slope region of the tail of a vG model increased the surface area and thus dissolution trapping in homogeneous reservoirs. The type of heterogeneity investigated here increased dissolution trapping to a much greater extent than did changes to the slope region of the vG tail.

The explanation of these differences between the BC and vG approaches is as follows. The rate of dissolution in a homogeneous reservoir is proportional to the CO_2-brine contact area. In the vG case, the contact area is diffuse and CO_2-brine boundary is wider than in the BC case. This is because there is a pore network with negligible capillary entry pressure in the vG case, which allows CO_2 to penetrate higher into the brine-saturated rock through this network. The same explanation is applicable for the heterogeneous reservoirs. However, the boundaries between different materials (CG and FG rocks in our case) should be also considered. In heterogeneous media, CO_2 propagates along highly permeable clusters in addition to moving up

by buoyancy force. As a result, a part of the CO_2 (in our example all CO_2 in the gas phase) is trapped at the CG-FG boundaries (the capillary pinning effect in BC case and capillary retardation effect in vG case; Figure 11), because the buoyancy force is smaller than the capillary pressure force. The latter force prevents CO_2 from moving upward. The penetration width of CO_2 at the CG-FG boundary depends on the pore-size distribution in FG rocks. The wider the distribution is the larger the effective CO_2-brine surface, and the larger the dissolution rate, which explains the results depicted in Figure 9. This effect on the dissolution rate is much larger in heterogeneous reservoirs than in homogeneous reservoirs because the total effective contact area is much larger in the latter case.

Capillary trapping (snap-off) in the homogeneous simulations was not sensitive to the type of capillary pressure curve; the capillary trapping rate and the amount are the same for BC and vG curves (Figure 8). In heterogeneous reservoirs, the CO_2-brine interface zone partially coincides with CG-FG boundaries (Figure 12). In this case, the width of the CO_2-brine interface zone affects the distribution of CO_2 between CG and FG rocks. In the BC approach, the width of the interface zone is smaller and CO_2 does not penetrate up into FG rocks. In contrast, in the vG approach, a part of the CO_2 penetrates into FG rocks. As a result, the ratio between amounts of CO_2 in FG rocks to amounts of CO_2 in CG rocks is larger in the vG approach. This explains why the amount of snap-off CO_2 is larger in FG rocks (and is smaller in CG rocks, respectively) in the vG approach than in the BC approach (Figure 12). Because the snap-off is larger in FG rocks than in CG rocks (per unit volume of material), the total amount of snap-off CO_2 in the entire (heterogeneous) reservoir is larger in the vG approach (Figure 8).

The effect described above, i.e., strong dependency of CO_2 trapping on the type of capillary pressure curve used for simulation, depends on CO_2 relative permeability curves as well. Difference between the amounts of snap-off in the vG and BC cases depends on the residual CO_2 saturation parameter. In cases where only a drainage curve is used for simulation and residual CO_2 saturation equals zero, snap-off trapping is absent. Calculated snap-off amount depends on the type of hysteresis model for history-dependent relative permeability functions used for simulation. The comparison between three models, i.e., Killough's [27], Carlson's [9] and Jargon's [45] models, showed that, for the conditions considered here, the difference may reach 20% between Killough's and Carlson's models and 50% between Killough's and Jargon's models.

The amount of CO_2 trapped by snap-off in the vG case depends on the tail shape, i.e., S_{nt} value; the larger is S_{nt}, the larger is the snap-off. This is because the larger tail allows more CO_2 to penetrate the FG rocks and thus more total (in both FG rocks and CG rocks rocks) CO_2 is trapped. However, the change in the trapping amount due to "tail size" is small compared to the change in the trapping due to switching from the vG to BC case.

Note that the grid-cell size used for simulation (2 × 2 × 0.05 m) was dictated by the typical size of the first (smallest) level of heterogeneity in geocellular model architecture [17, 50]. This size was established based on field measurements of fluvial depositions [3, 42-44]. An increase in grid-cell size will cause the loss or corruption of this level of heterogeneities. This will lead to erroneous results because most of the effects described here occur because of the presence of small-scale heterogeneity. In particular, the connectivity of highly permeable rocks will be altered. However, small grid size does not allow simulation of CO_2 injection in realistically sized reservoirs with volumes a few orders of magnitude larger than the reservoir volume considered here. Upscaling requires averaging effects of small-scale heterogeneity, which is a subject of our further research.

The same general findings would be expected in other types of sedimentary architecture where coarser-grained rock types with lower entry pressures are juxtaposed within finer-grained rock types with higher entry pressures (e.g., eolian deposits with coarser- and finer-grained cross-sets or alluvial deposits with incised coarser-grained channel lags).

What capillary pressure curve best describes the behaviour of CO_2 in brine-filled, fluvial reservoirs? Li [36] noted that the BC approach has been used frequently for lithified porous media (rock) and the vG approach for unlithified porous media (soils). Indeed, the published data for reservoir rocks often indicate that the BC approach is appropriate, e.g., Krevor et al. [30]. There are reported attempts to combine the BC and vG approaches to one closed-form model based on the experimental data with a variety of rocks, e.g., [33, 36, 57]. Results of these studies indicate that, in some cases, both curve types fit experimental data equally well; in other cases, one of the types is more preferable than the other. The detailed comparison of six relative permeability–saturation–capillary-pressure models (two BC and four vG types) based on experimental data with sandstones from four different formations was recently implemented by Oostrom et al. [48]. Only processes during injection were analyzed in one-dimensional and two-dimensional homogeneous reservoirs in that study. Even with these limitations, the results show

large variations in plume shape and CO_2 saturation distribution depending on the model used. Those results and the results of our study suggest that a high priority should be given to quantifying the existence or absence of entry pressures, and, if present, their heterogeneity as a part of characterizing candidate fluvial reservoirs for CO_2 sequestration.

But this is one part of the problem. The second part is the implementation of the BC approach in simulation software. Widely used simulation packages, such as TOUGH2, do not implement the BC approach for capillary pressure. Though ECLIPSE does implement this approach, there are essential differences between the BC and vG cases: (1) calculation time is one to two orders of magnitude larger in the former case; and (2) there are more convergence problems in the BC case. The future versions of these and other software should include algorithms with a sufficiently implemented BC option for capillary pressure curves, e.g., [35, 37, 38].

Acknowledgements

We thank the Editor and reviewers for comments and suggestions used to improve this manuscript. This work was supported as part of the Center for Geological Storage of CO_2, an Energy Frontier Research Center funded by the U.S. Department of Energy, Office of Science, Basic Energy Sciences under Award # DE-SC0C12504. We acknowledge Schlumberger Limited for the donation of ECLIPSE Reservoir Simulation Software. We thank Daniel Klen for manuscript editing. Both the data and input files necessary to reproduce the simulations are freely available from the authors upon request (naum.gershenzon@wright.edu).

REFERENCES

[1] Altundas, Y.B., T.S. Ramakrishnan, N. Chugunov, and R. de Loubens (2011), Retardation of CO_2 Caused by Capillary Pressure Hysteresis: A New CO_2 Trapping Mechanism, *SPE Journal*, 16 (4), 784–794, doi: http://dx.doi.org/10.2118/139641-PA.

[2] Boait F, White N, Chadwick A, Noy D, Bickle M. Layer spreading and dimming within the CO2 plume at the Sleipner field in the North Sea. Energy Procedia 2011; 4: 3254–61. http://dx.doi.org/10.1016/j.egypro.2011.02.244.

[3] Bridge, J.S. (2006), Fluvial facies models: Recent developments, in Facies Models Revisited, SEPM Spec. Publ., 84, edited by H. W. Posamentier and R. G. Walker, 85–170, Soc. for Sediment. Geol. (SEPM), Tulsa, Okla.

[4] Brooks, R. J., and A. T. Corey (1964), Hydraulic properties of porous media, Hydrol. Pap. 3, Colo. State Univ., Fort Collins.

[5] Bryant, S. L., S. Lakshiminarasimhan, and G. A. Pope (2006), Buoyancy-dominated multiphase flow and its impact on geological sequestration of CO_2, SPE 99938, SPE/DOE Symposium on Improved Oil Recovery, Tulsa, Okla.

[6] Dance, T. (2009), A workflow for storage site characterization, A case study from the CO2CRC Otway Project, AAPG/SEG/SPE Hedberg Conference on Geological Carbon Sequestration and Verification, August 16–19, Vancouver BC.

[7] Delshad, M., X. Kong, R. Tavakoli, S.A. Hosseini, and M.F. Wheeler (2013), Modeling and simulation of carbon sequestration at Cranfield incorporating new physical models, *Int. J. Greenhouse Gas Control*, 18, 463–473, doi: 10.1016/j.ijggc.2013.03.019.

[8] Dullien, F.A.L. (1992), Porous Media Fluid Transport and Pore Structure, Academic, San Diego.

[9] Carlson, F.M. (1981), Simulation of Relative Permeability Hysteresis to the Nonwetting Phase. Presented at the *SPE Annual Fall Technical Conference and Exhibition*, San Antonio, Texas, USA, SPE-10157-MS. http://dx.doi.org/10.2118/10157-MS.

[10] Ide, S.T., Jessen K, Orr Jr FM. (2007) Storage of CO_2 in saline aquifers: Effects of gravity, viscous, and capillary forces on amount and timing of trapping. *Int. J Greenhouse Gas Control*. 1, 481–91.

[11] Fenghour, A., Wakeham, W.A., Vesovic, V. (1998) The Viscosity of Carbon Dioxide. *J. Phys. Chem. Ref. Data*, 27, 1, 31–44.

[12] Flett, M., R. Gurton, and G. Weir (2007), Heterogeneous saline formations for carbon dioxide disposal: Impact of varying heterogeneity on containment and trapping, *J. Pet. Sci. Eng.*, 57, 106–118, doi: 10.1016/j.petrol.2006.08.016.

[13] Freiburg, J., D. Morse, H. Leetaru, R. Hoss, and Q. Yan (2014), A depositional and diagenetic characterization of the Mt. Simon Sandstone at the Illinois Basin–Decatur Project Carbon Capture and Storage Site, Decatur, Illinois, USA, Circular 583, Illinois State Geological Survey, University of Illinois, Urbana-Champaign.

513 [14] Gale, J., J.C. Abanades, S. Bachu and C. Jenkins, 2015, Special Issue commemorating the
514 10th year anniversary of the publication of the Intergovernmental Panel on Climate Change
515 Special Report on CO_2 Capture and Storage, International Journal of Greenhouse Gas Control 40
516 (2015) 1–5, doi.org/10.1016/j.ijggc.2015.06.019.
517 [15] Gershenzon, N. I., M.R. Soltanian , R. W. Ritzi Jr, D.F. Dominic, E. Mehnert, R.T. Okwen
518 (2015) Influence of Small-Scale Fluvial Architecture on CO_2 Trapping Processes in Deep Brine
519 Reservoirs, Water Resour. Res., 51, 8240–8256, doi:10.1002/2015WR017638.
520 [16] Gershenzon, N. I., M.R. Soltanian , R. W. Ritzi Jr, D.F. Dominic, (2014) Influence of small
521 scale heterogeneity on CO_2 trapping processes in deep saline aquifers. *Energy Procedia* 59, 166–
522 73.
523 [17] Guin, A., R. Ramanathan, R. W. Ritzi Jr., D. F. Dominic, I. A. Lunt, T. D. Scheibe, and V.
524 L. Freedman (2010), Simulating the heterogeneity in braided channel belt deposits: 2. Examples
525 of results and comparison to natural deposits, *Water Resour. Res.*, 46, W04516,
526 doi:10.1029/2009WR008112.
527 [18] Han, W. S., S.-Y. Lee, C. Lu, and B. J. McPherson (2010), Effects of permeability on CO_2
528 trapping mechanisms and buoyancy-driven CO_2 migration in saline formations, *Water Resour.*
529 *Res.*, 46, W07510, doi:10.1029/2009WR007850.
530 [19] Holtz, M.H. (2002), Residual Gas Saturation to Aquifer Influx: A Calculation Method for 3-
531 D Computer Reservoir Model Construction, paper was prepared for presentation at the SPE Gas
532 Technology Symposium held in Calgary, Alberta, Canada, 30 April–2 May 2002.
533 [20] Hovorka S.D., C. Doughty, S. M. Benson, K. Pruess and P.R. Knox (2004), The impact of
534 geological heterogeneity on CO_2 storage in brine formations: a case study from the Texas Gulf
535 Coast. Geological Society, London, Special Publications, 233, 147–163.
536 [21] Hunt, J. R., N. Sitar, and K. S. Udell (1988), Nonaqueous phase liquid transport and
537 cleanup: 1. Analysis of mechanisms, *Water Resour. Res.*, 24(8), 1247–1258.
538 [22] Ide, S.T., K. Jessen, F.M. Orr Jr. (2007), Storage of CO_2 in saline aquifers: Effects of
539 gravity, viscous, and capillary forces on amount and timing of trapping, *International Journal of*
540 *Greenhouse Gas Control*, 1(4), 481 – 491, doi: 10.1016/S1750-5836(07)00091-6.
541 [23] Iglauer, S., C. H. Pentland, and A. Busch (2015), CO_2 wettability of seal and reservoir rocks
542 and the implications for carbon geo-sequestration, *Water Resour. Res.*, 51, 729–774,
543 doi:10.1002/2014WR015553.

[24] Iglauer, S., A. Paluszny, C. H. Pentland, and M.J.Blunt (2011), Residual CO_2 imaged with X-ray micro-tomography, *Geophys. Res. Lett.*, 38, L21403, doi:10.1029/2011GL049680.

[25] Joekar-Niasar, V., F. Doster, R.T. Armstrong, D. Wildenschild, and M.A. Celia, (2013), Trapping and hysteresis in two-phase flow in porous media, *Water Resources Research*, 49, 1–13, doi:10.1002/wrcr.2031.

[26] Juanes, R., E. J. Spiteri, F. M. Orr Jr., and M. J. Blunt (2006), Impact of relative permeability hysteresis on geological CO_2 storage, *Water Resour. Res.*, 42, W12418, doi:10.1029/2005WR004806.

[27] Killough, J. E. (1976) Reservoir Simulation with History-dependent Saturation Functions *Trans. AIME* 261, 37–48.

[28] Kopp A, H. Class, and R. Helmig (2009), Investigations on CO_2 storage capacity in saline aquifers. Part 1: Dimensional analysis of flow processes and reservoir characteristics. *Int J Greenhouse Gas Control*, 3, 263–76.

[29] Krevor, S.C., R. Pini, B. Li, and S. M. Benson (2011), Capillary heterogeneity trapping of CO_2 in a sandstone rock at reservoir conditions, Geophys. Res. Lett., 38, L15401, doi:10.1029/2011GL048239.

[30] Krevor, S.C., R. Pini, L. Zuo, and S. M. Benson (2012), Relative permeability and trapping of CO_2 and water in sandstone rocks at reservoir conditions, *WaterResour.Res*, 48 , W02532, doi:10.1029/2011WR010859.

[31] Krevor, S.C, M.J. Blunt, S.M. Benson, C.H. Pentland, C. Reynolds, A. Al-Menhali, B. Niu (2015), Capillary trapping for geologic carbon dioxide storage –From pore scale physics to field scale implications, *International Journal of Greenhouse Gas Control*, 40, 221–237, doi.org/10.1016/j.ijggc.2015.04.006.

[32] Kumar, A., R. Ozah, M. Noh, G. A. Pope, S. Bryant, K. Sepehrnoori, and L.W. Lake (2005), Reservoir simulation of CO_2 storage in deep saline aquifers, *SPE Journal*, 10(3), 336–348, doi: http://dx.doi.org/10.2118/89343-PA.

[33] Leij F, RusselW, Lesch S (1997) Closed-form expressions for water retention and conductivity data. Ground Water 35(5):848–858, 10.1111/j.1745-6584.1997.tb00153.x.

[34] Lenhard R, J. Parker, S. Mishra (1989), On the correspondence between Brooks-Corey and van Genuchten models. *Journal of Irrigation and Drainage Engineering*. 115, 744–751 doi: 10.1061/(ASCE)0733-9437(1989)115:4(744).

575 [35] Lichtner, P.C., G.E. Hammond, C. Lu, S. Karra, G. Bisht, B. Andre, R. Mills, J. Kumar,
576 (2015) PFLOTRAN User Manual.
577 [36] Li, K., (2010), More general capillary pressure and relative permeability models from
578 fractal geometry. *Journal of Contaminant Hydrology* 111, 13–24.
579 [37] Li B. Including fine-scale capillary heterogeneity in modeling the flow of CO_2 and brine in
580 reservoir cores. M.S. thesis, Stanford University, USA; 2011.
581 [38] Li B, Benson SM, Tchelepi HA. Modeling fine-scale capillary heterogeneity in multiphase
582 flow of CO_2 and brine in sedimentary rocks. In: Proceedings of the XIX international conference
583 on water resources University of Illinois at Urbana-Champaign, IL, USA; June 2012. p. 17–22.
584 [39] Li, B., H. A. Tchelepi , S.M. Benson (2013), Influence of capillary-pressure models on CO_2
585 solubility trapping, *Advances in Water Resources*, 62(C): 488–98, doi:
586 0.1016/j.advwatres.2013.08.005.
587 [40] Li, B., & S.M. Benson, (2015). Influence of small-scale heterogeneity on upward CO_2
588 plume migration in storage aquifers. Advances in Water Resources, 83, 389–404.
589 [41] Lu, J., R. Reed, and S. Hovorka (2011), Diagenesis and sealing capacity of the middle
590 Tuscaloosa mudstone at the Cranfield carbon dioxide injection site, Mississippi, U.S.A.,
591 *Environmental Geosciences*, 18(1), 35–53, doi:10.1306/eg.09091010015.
592 [42] Lunt, I.A. and J.S. Bridge (2007), Formation and preservation of open framework gravel
593 strata in unidirectional flows, *Sedimentology*, 54, 71–87, doi:10.1111/j.1365-3091.2006.00829.x.
594 [43] Lunt, I.A., J.S. Bridge, and R.S. Tye (2004), A quantitative, three dimensional depositional
595 model of gravelly braided rivers, *Sedimentology*, 51(3), 377–414, doi:10.1111/j.1365-
596 3091.2004.00627.x.
597 [44] Lunt, I.A. (2002), A three-dimensional, quantitative depositional model of gravelly braided
598 river sediments with special reference to the spatial distribution of porosity and permeability,
599 Phd dissertation, Binghamton University, State University of New York.
600 [45] Manual “ECLIPSE reservoir simulation software, Technical Description”, Version 2010.2
601 [46] Meckel TA, Bryant SL, Ganesh PR. (2015), Characterization and prediction of CO_2
602 saturation resulting from modeling buoyant fluid migration in 2D heterogeneous geologic
603 fabrics. *International Journal of Greenhouse Gas Control*, 34, 85–96.

[47] Mo, S., P. Zweigel, E. Lindeberg, and I. Akervoll (2005), Effect of geologic parameters on CO_2 storage in deep saline aquifer, *The 14th Europec Biennial Conference*, Madrid, Spain, SPE 93952.

[48] Oostroma, M.D. White, S.L. Porse, S.C.M. Krevor, S.A. Mathias (2016), Comparison of relative permeability–saturation–capillary pressuremodels for simulation of reservoir CO2injection. *International Journal of Greenhouse Gas Control*, 45, 70–85.

[49] Pini, R., S.C. Krevor, and S. M. Benson, 2012. Capillary pressure and heterogeneity for the CO_2/water system in sandstone rocks at reservoir conditions, Advances in Water Resources 38 (2012) 48–59.

[50] Ramanathan, R., A. Guin, R. W. Ritzi Jr., D. F. Dominic, V. L. Freedman, T. D. Scheibe, and I. A. Lunt (2010), Simulating the heterogeneity in braided channel belt deposits: 1. A geometric-based methodology and code, *Water Resour. Res.*, 46, W04515, doi:10.1029/2009WR008111.

[51] Ritzi, R.W., J.T. Freiburg, N.D. Webb, (2016), Understanding the (co)variance in petrophysical properties of CO_2 reservoirs comprising fluvial sedimentary architecture, *International Journal of Greenhouse Gas Control*, (51), p. 423-434, doi: 10.1016/j.ijggc.2016.05.001

[51] Saadatpoor, E., Steven L. Bryant, and K. Sepehrnoori (2009), Effect of capillary heterogeneity on buoyant plumes: A new local trapping mechanism, *Energy Procedia*, 1(1), 3299–3306,doi: 10.1016/j.egypro.2009.02.116.

[52] Spycher, N. and K. Pruess (2005) CO_2-H_2O mixtures in the geological sequestration of CO2.II. Partitioning in chloride brines at 12-100 C and up to 600 bar. *Geochimica et Cosmochimica Acta*, 69 (13), 3309–3320.

[53] Spiteri, E. J., R. Juanes, M. J. Blunt, and F. M. Orr (2008), A new model of trapping and relative permeability hysteresis for all wettability characteristics, *SPE Journal*, 13(3), 277–288 doi: http://dx.doi.org/10.2118/96448-PA.

[54] Trevisan L., R. Pini, A. Cihan, J.T. Birkholzer, Q. Zhou, and T.H. Illangasekare (2015) Experimental analysis of spatial correlation effects on capillary trapping of supercritical CO_2 at the intermediate laboratory scale in heterogeneous porous media. doi: 10.1002/2015WR017440

[55] Tye, R. S., B. A. Watson, P. L. McGuire, and M. M. Maguire (2003), Unique horizontal-well designs boost primary and EOR production, Prudhoe Bay field, Alaska, in T. R. Carr, E. P.

Mason, and C. T. Feazel, eds., Horizontal wells: Focus on the reservoir: AAPG Methods in Exploration, 14, 113–125.

[56] van Genuchten M.T. (1980), A closed-form equation for predicting the hydraulic conductivity of unsaturated soils. *Soil Sci Soc Am J*, 44(5), 892–8.

[57] Valiantzas, J.D. (2011) Combined Brooks-Corey/Burdine and van Genuchten/Mualem Closed-Form Model for Improving Prediction of Unsaturated Conductivity. *Journal of Irrigation and Drainage Engineering*, 137(4), 223–233.

[58] Vesovic, V. Wakeham, W. A., Olchowy, G.A., Sengers, J.V., Watson, J.T.R., Millat, J. (1990), The Transport Properties of Carbon Dioxide. *J. Phys. Chem. Ref. Data*, 19, 3, 763–808.

[59] Wildenschild, D., R.T. Armstrong, A.O. Herring, I.M. Young, and J.W. Carey (2011) Exploring capillary trapping efficiency as a function of interfacial tension, viscosity, and flow rate, *Energy Procedia* 4, 4945–4952, doi:10.1016/j.egypro.2011.02.464.

[60] Zhou, Q., Birkholzer, J. T., Mehnert, E., Lin, Y.F. and Zhang, K. (2010), Modeling Basin- and Plume-Scale Processes of CO_2 Storage for Full-Scale Deployment, *Groundwater*, 48(4), 494–514, doi: 10.1111/j.1745-6584.2009.00657.x.

Figures legends

Figure 1. (a) Snap-off trapping: Counter-imbibition of brine (the wetting fluid) behind the advancing plume occurs preferentially through smaller pores and pore throats, trapping CO_2 bubbles within the intervening pore bodies (e.g., [22, 25, 62]). **(b)** Capillary pinning: CO_2 is pinned below local contacts between an underlying rock type with larger pores and an overlying rock type with smaller pores and thus larger entry pressure. This occurs where the entry pressure (P_e) of the FG rock exceeds the buoyant pressure (P_b) of CO_2 in the CG rock (e.g., [5, 16, 17, 23, 53, 63]); this effect is quasi-permanent. **(c)** Capillary retardation: a transient pinning effect in which CO_2 preferentially enters regions with larger pores during injection, and leaks through network of pores with negligibly small capillary pressure in the overlying, finer-grained rock. Increase in CO_2 saturation in the finer grained rock is rate-limited because of the difference in saturation relationships between rock types, retarding plume movement, as explained in Figure 2.

Figure 2. (a) Schematic illustration of 'capillary pinning' effect in BC case. If for a given CO_2 saturation, S_{CG}^{w}, capillary pressure in CG unit, $P_c(S_{CG}^{w})$, is less than the entry pressure in overlying $P_{e,FG}$ FG unit, $P_c(S_{FG}^{w}=1)\equiv P_{e,FG}$, minus the buoyant force per unit area, then CO_2 from CG unit is unable to penetrate to FG unit. **(b)** Schematic illustration of 'capillary retardation' effect in the vG case. As long as brine saturation in the FG unit exceeds S_{FG}^{w}, some

amount of buoyant CO_2 may freely penetrate the overlying rock without any capillary pressure barrier. However, because CO_2 will not enter the overlying unit when P_c in the overlying rock exceeds $P_c(S_{CG}^w)$, capillary pressure will limit the rate at which CO_2 saturation can increase in the overlying unit.

Figure 3. Fluvial forms and internal architecture, from Ritzi et al. [51]. (a) A modern fluvial channel-belt system comprising active channels and compound bars. The compound bars, in turn, comprise unit bars. (b) Conceptual diagram of a compound bar with unit bars outlined in green. (c) Cross section through (b) showing that unit bar deposits comprise sets of cross strata with different textures. .

Figure 4. Rendering of the geocellular model populated with intrinsic permeability. The CG cross-sets (24% by volume) are apparent as higher-permeability regions. Paleoflow was right to left, and thus the CG cross-sets dip to the left. Though boundaries of unit bar deposits cannot be easily distinguished in this rendering, the cross-sets dip more steeply at the front of unit bar deposits and these differences in dip are apparent. Vertical exaggeration is 10×.

Figure 5. Capillary pressure (a), relative permeability of CO_2 (b) and relative permeability of water (c) in FG and CG rocks for drainage and imbibition.

Figure 6. Brooks-Corey (equation (8)) and van Genuchten-type (equation (9)) capillary pressure curves for CG and FG rocks for drainage.

Figure 7. Vertical cross section of a homogeneous reservoir showing CO_2 saturation after 1,010 days (1,000 days after the end of injection) in simulations using the vG (top panel) and BC (bottom panel) approaches for capillary pressure curves. Vertical exaggeration is 10×.

Figure 8. The dynamics of CO_2 trapping (fraction from the total amount of injected CO_2) in homogeneous and heterogeneous reservoirs in simulations using the BC and vG approaches for capillary pressure curves.

Figure 9. The dynamics of CO_2 (fraction from the total amount of injected CO_2) dissolved in homogeneous and heterogeneous reservoirs in simulations using the BC and vG approaches for capillary pressure curves.

Figure 10. The dynamics of supercritical CO_2 (fraction from the total amount of injected CO_2) in homogeneous and heterogeneous reservoirs in simulations using BC and vG approaches for capillary pressure curves. At large time this “mobile” CO_2 is actually trapped by entry-pressure pinning in the heterogeneous BC case, and by reaching the top of the domain in both homogeneous cases.

Figure 11. Vertical cross section of a heterogeneous reservoir showing CO_2 saturation after 1,010 days (1,000 days after the end of injection) in simulations using the vG approach (top panel) and BC approach (bottom panel) for capillary pressure curves. Vertical exaggeration is 10×.

Figure 12. The dynamics of CO_2 trapping by snap-off (fraction from the total amount of injected CO_2) in heterogeneous reservoirs using the BC and vG approaches for capillary pressure curves.

Figure 13. Three-dimensional images of a heterogeneous reservoir showing CO_2 saturation after 7.5, 110, and 10,000 days with snap-off trapping suppressed, using the BC (left) and vG (right) approaches for capillary pressure curves. Vertical exaggeration is 8×.

Figure 1

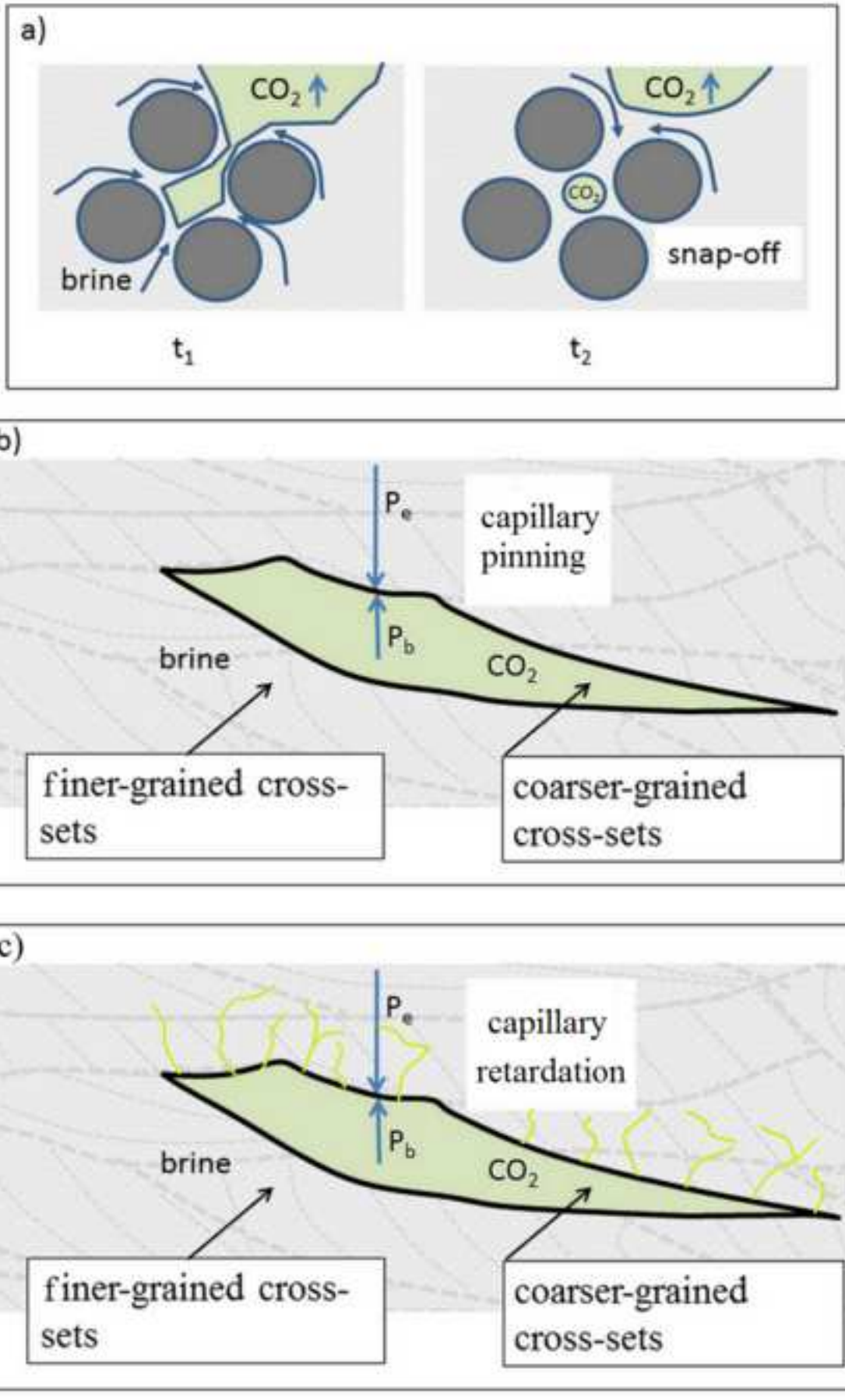
a)
CO_2
brine
t_1
CO_2
CO_2
snap-off
t_2
b)
P_e
capillary pinning
P_b
brine
CO_2
finer-grained cross-sets
coarser-grained cross-sets
c)
P_e
capillary retardation
P_b
brine
CO_2
finer-grained cross-sets
coarser-grained cross-sets

Figure 2

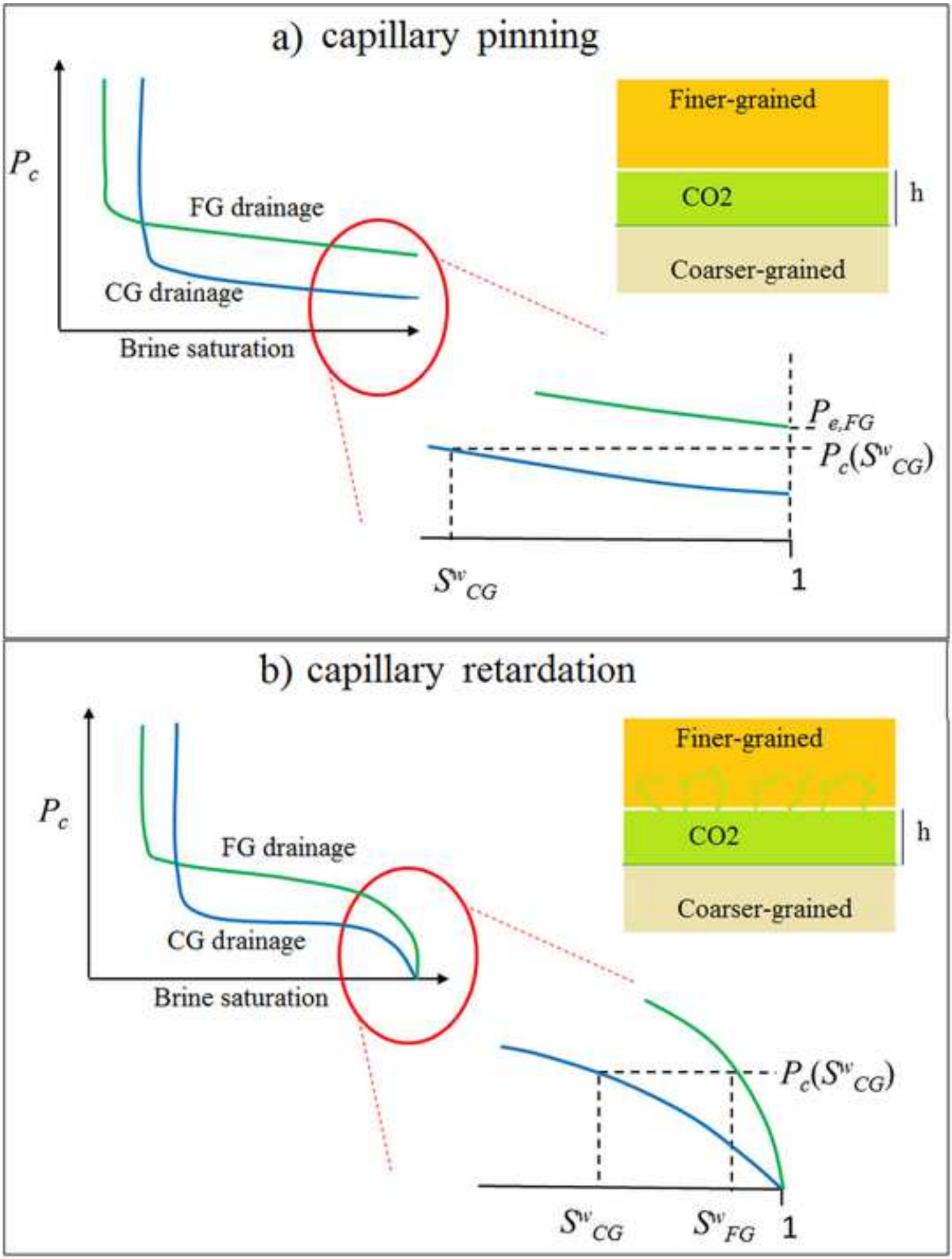
a) capillary pinning
P_c
FG drainage
CG drainage
Brine saturation
Finer-grained
CO2
h
Coarser-grained
$P_{e,FG}$
$P_c(S^w_{CG})$
S^w_{CG}
1
b) capillary retardation
P_c
FG drainage
CG drainage
Brine saturation
Finer-grained
CO2
h
Coarser-grained
$P_c(S^w_{CG})$
S^w_{CG}
S^w_{FG}
1

Figure 3

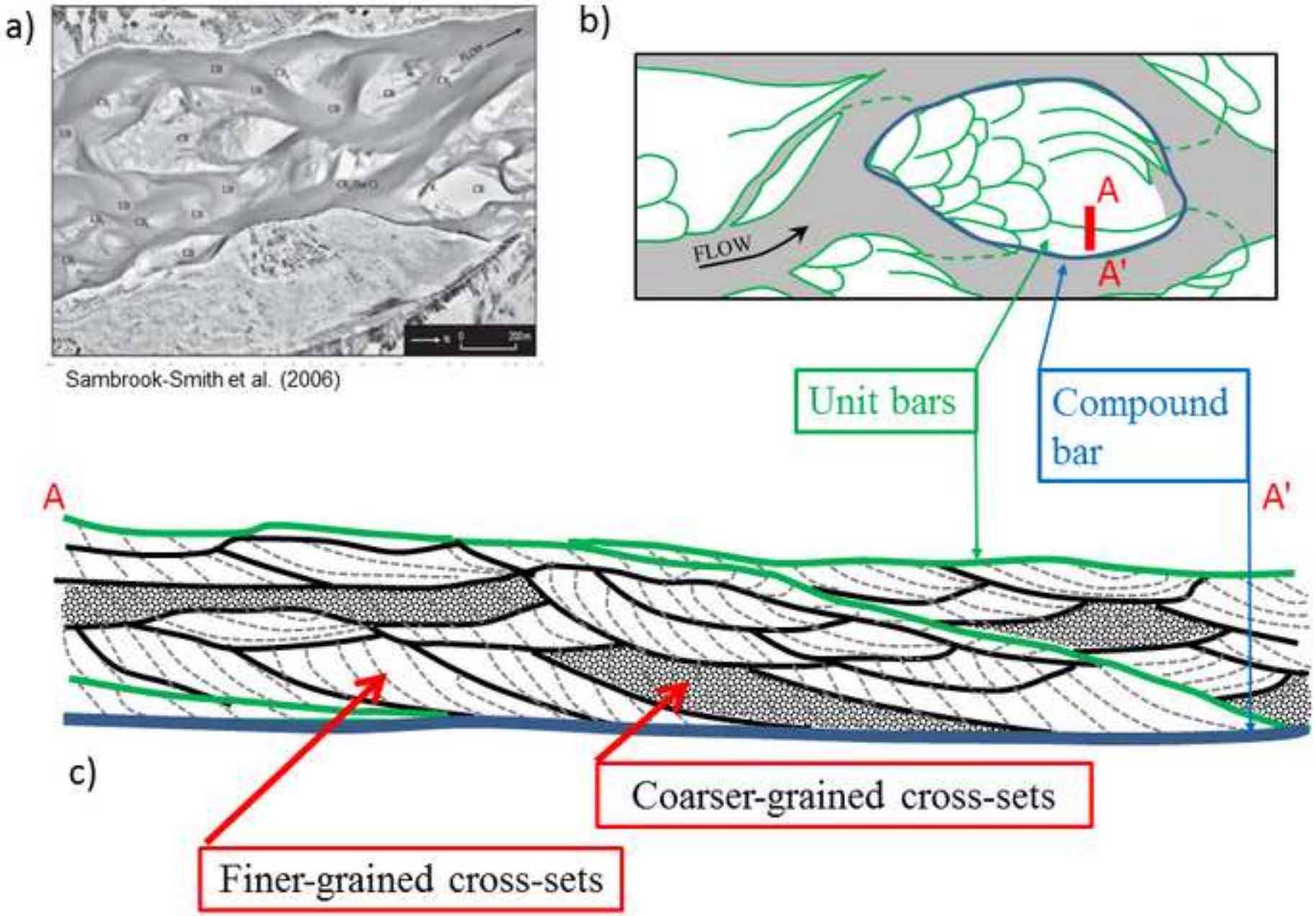
a)
Sambrook-Smith et al. (2006)
b)
FLOW
A
A'
Unit bars
Compound bar
A
A'
c)
Coarser-grained cross-sets
Finer-grained cross-sets

Figure 4

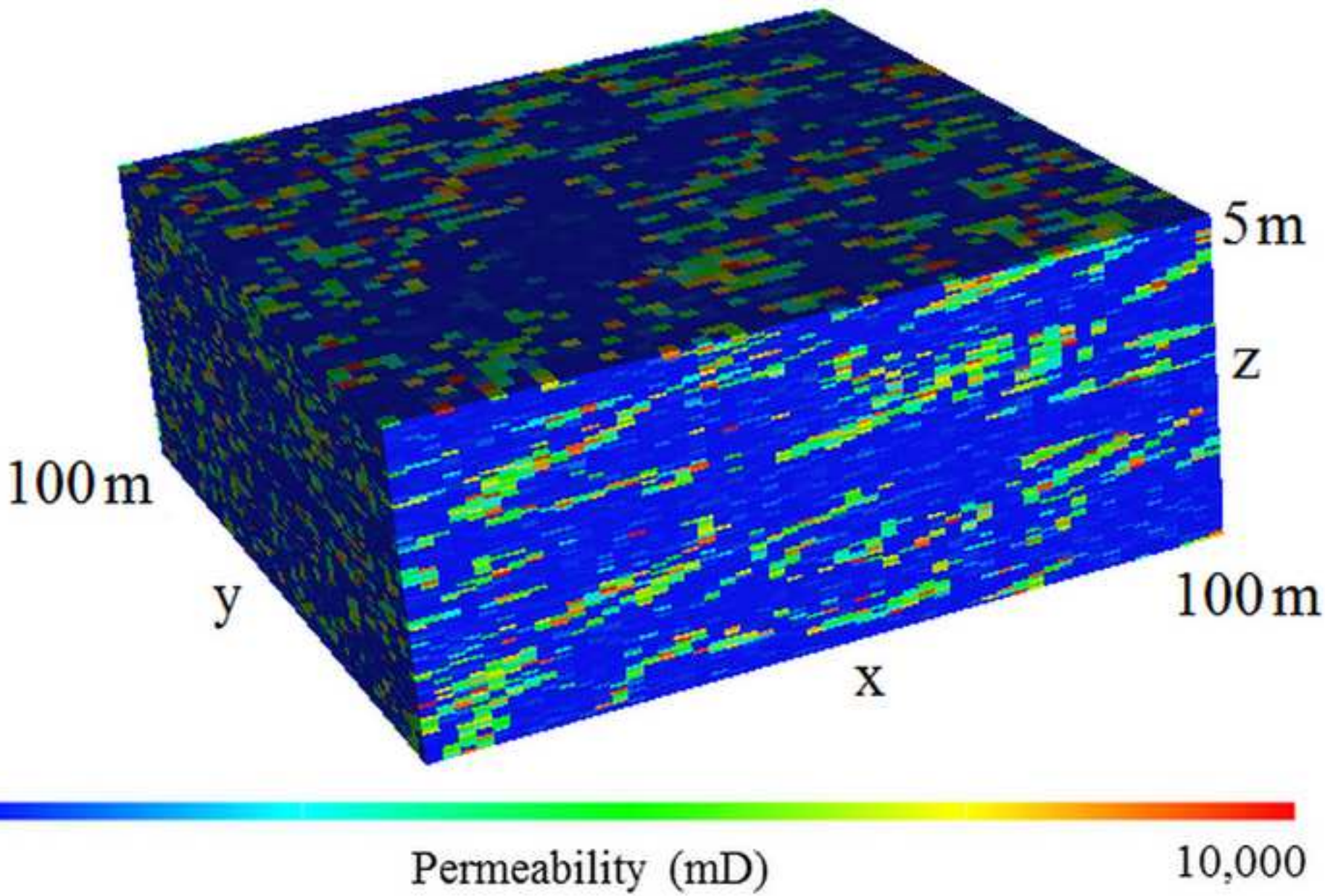

Figure 5

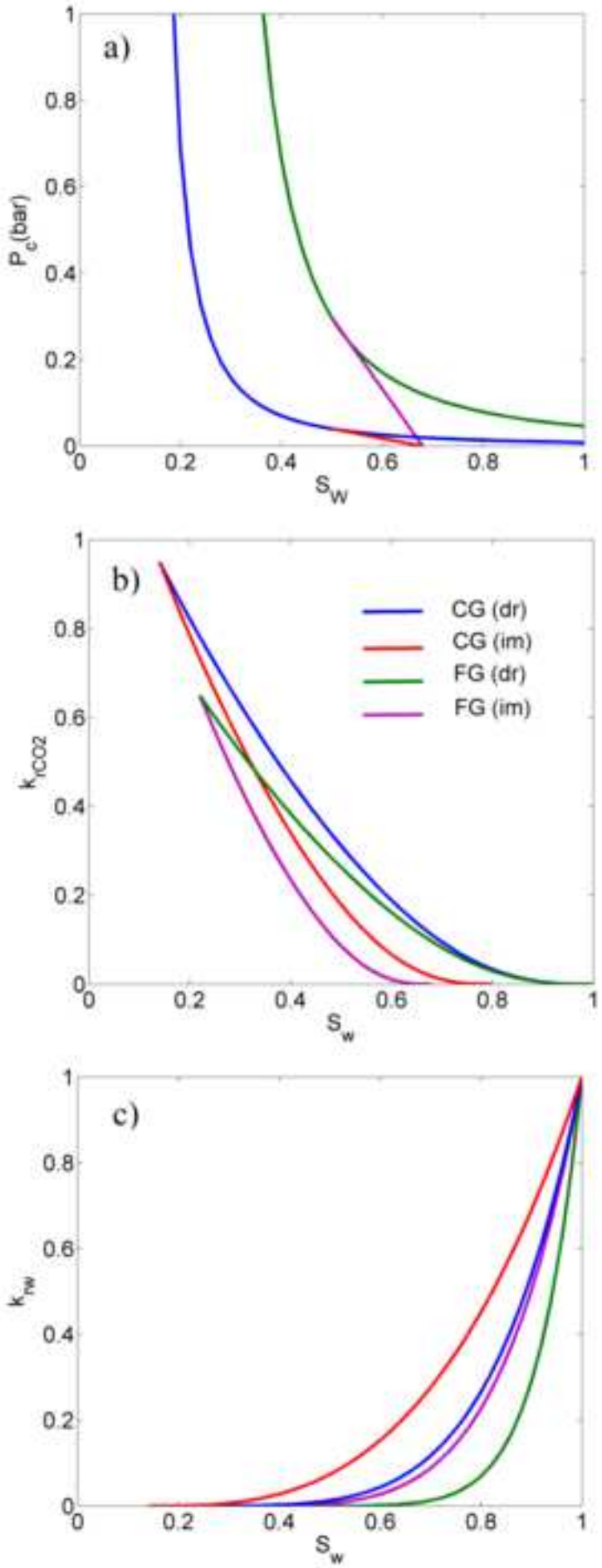

Figure 6

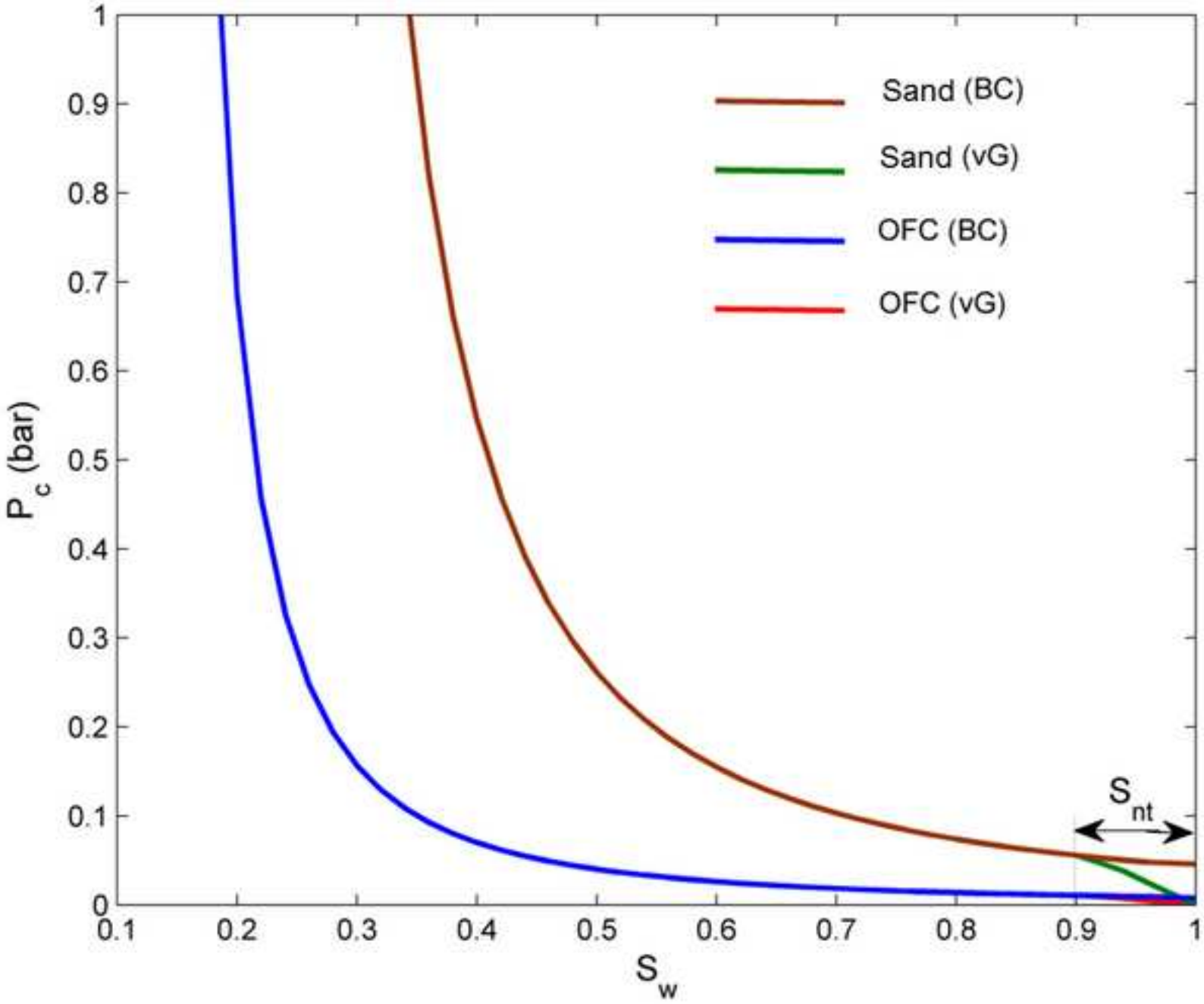
Sand (BC)
Sand (vG)
OFC (BC)
OFC (vG)
S_{nt}
P_c (bar)
S_w
0
0.1
0.2
0.3
0.4
0.5
0.6
0.7
0.8
0.9
1

Figure 7

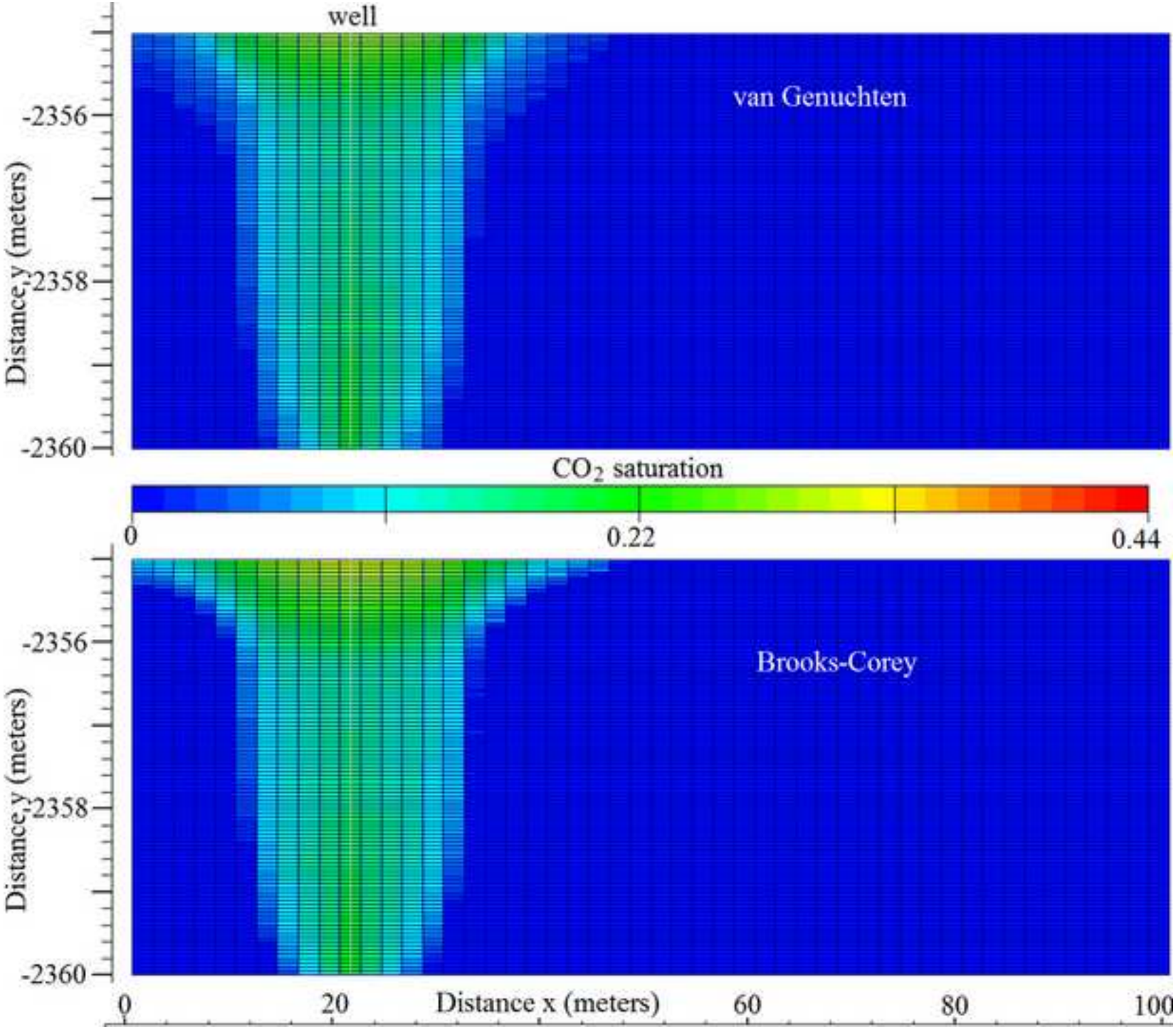
well
van Genuchten
-2356
-2358
-2360
Distance y (meters)
CO_2 saturation
0
0.22
0.44
Brooks-Corey
-2356
-2358
-2360
Distance y (meters)
0
20
Distance x (meters)
60
80
100

Figure 8

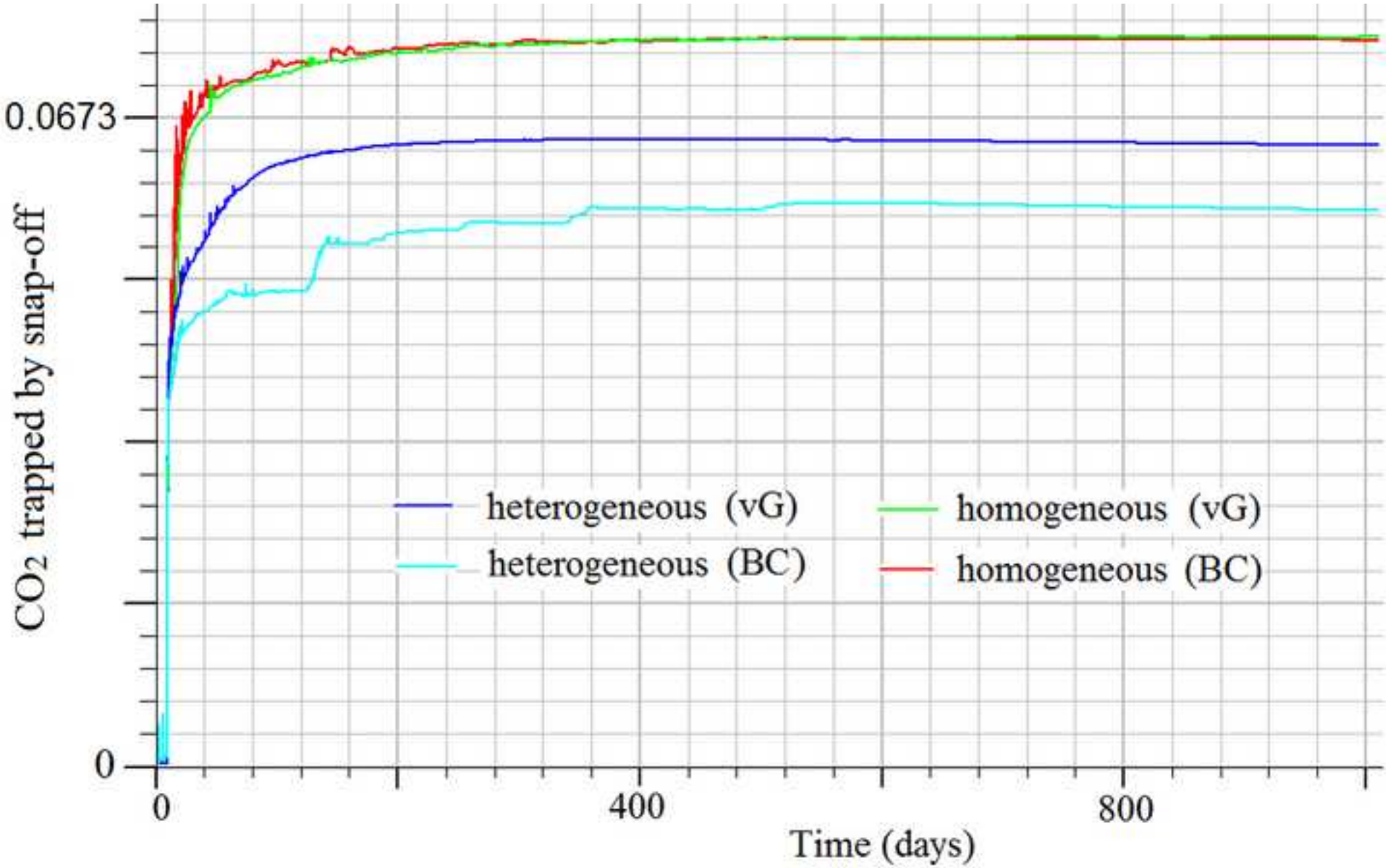
0.0673
0
CO_2 trapped by snap-off
heterogeneous (vG)
heterogeneous (BC)
homogeneous (vG)
homogeneous (BC)
0
400
800
Time (days)

Figure 9

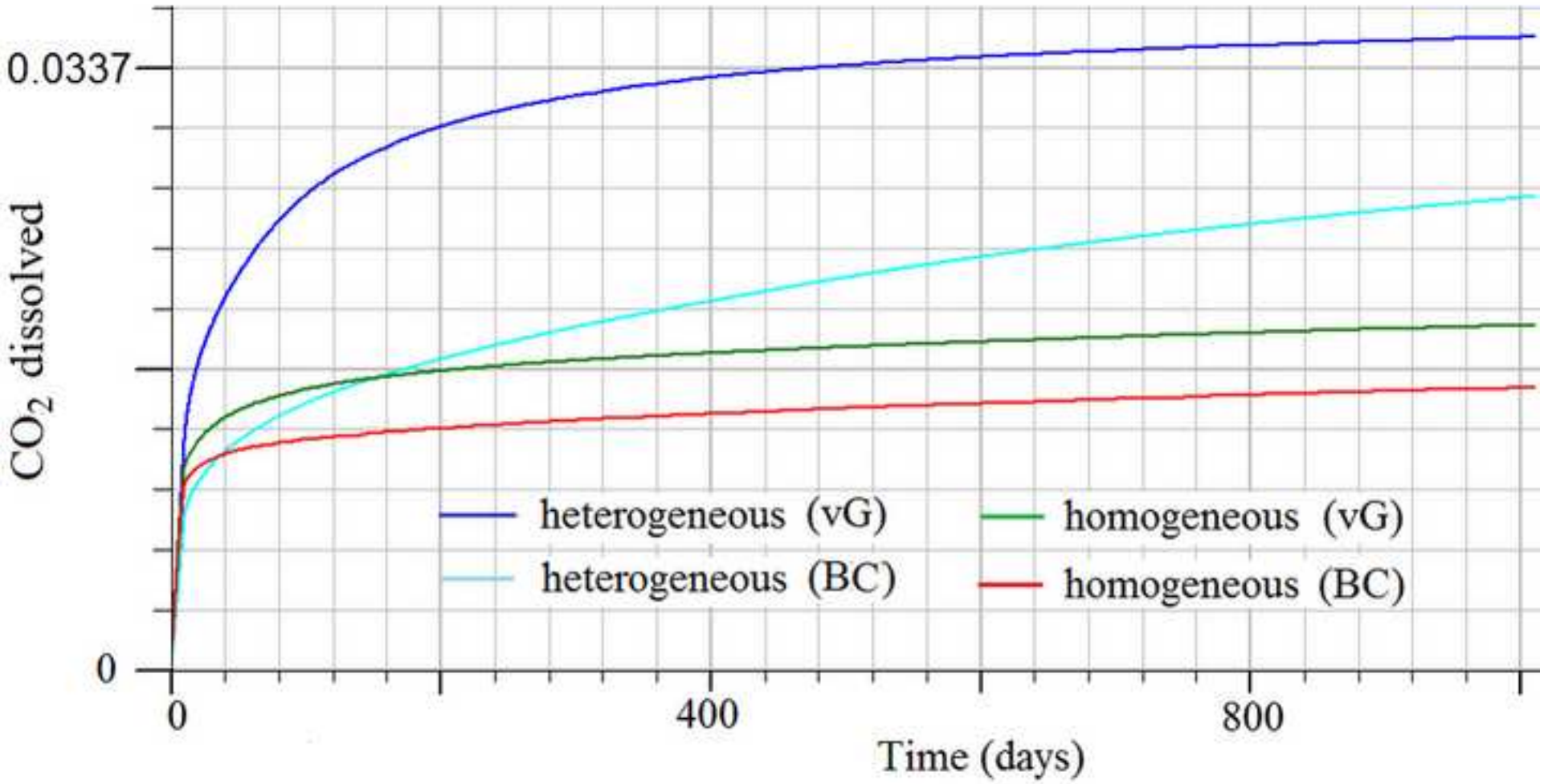
0.0337
0
CO_2 dissolved
heterogeneous (vG)
heterogeneous (BC)
homogeneous (vG)
homogeneous (BC)
0
400
800
Time (days)

Figure 10

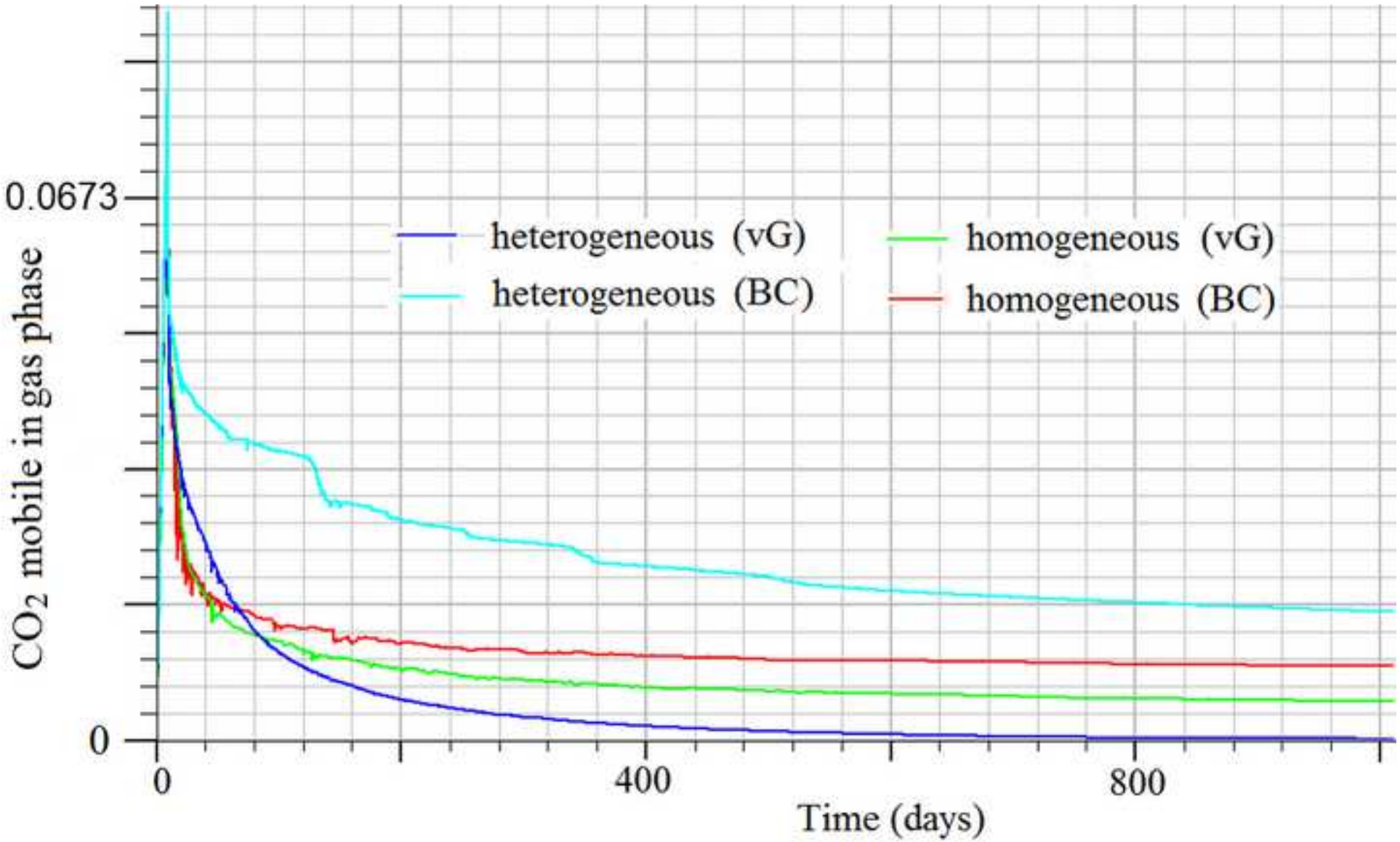
0.0673
0
CO_2 mobile in gas phase
heterogeneous (vG)
heterogeneous (BC)
homogeneous (vG)
homogeneous (BC)
0
400
800
Time (days)

Figure 11

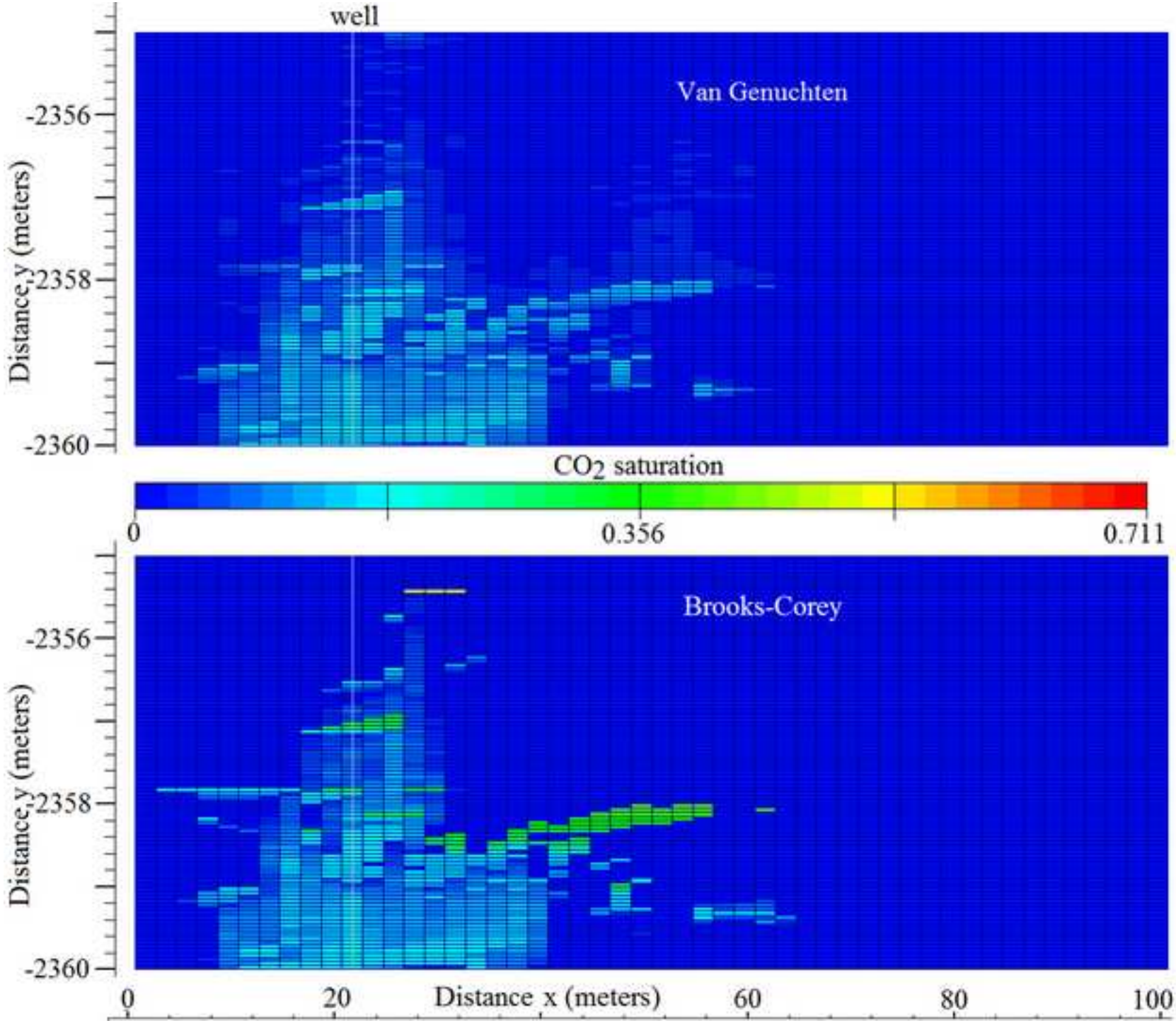
well
Van Genuchten
-2356
-2358
-2360
Distance,y (meters)
CO_2 saturation
0
0.356
0.711
Brooks-Corey
-2356
-2358
-2360
Distance,y (meters)
0
20
Distance x (meters)
60
80
100

Figure 12

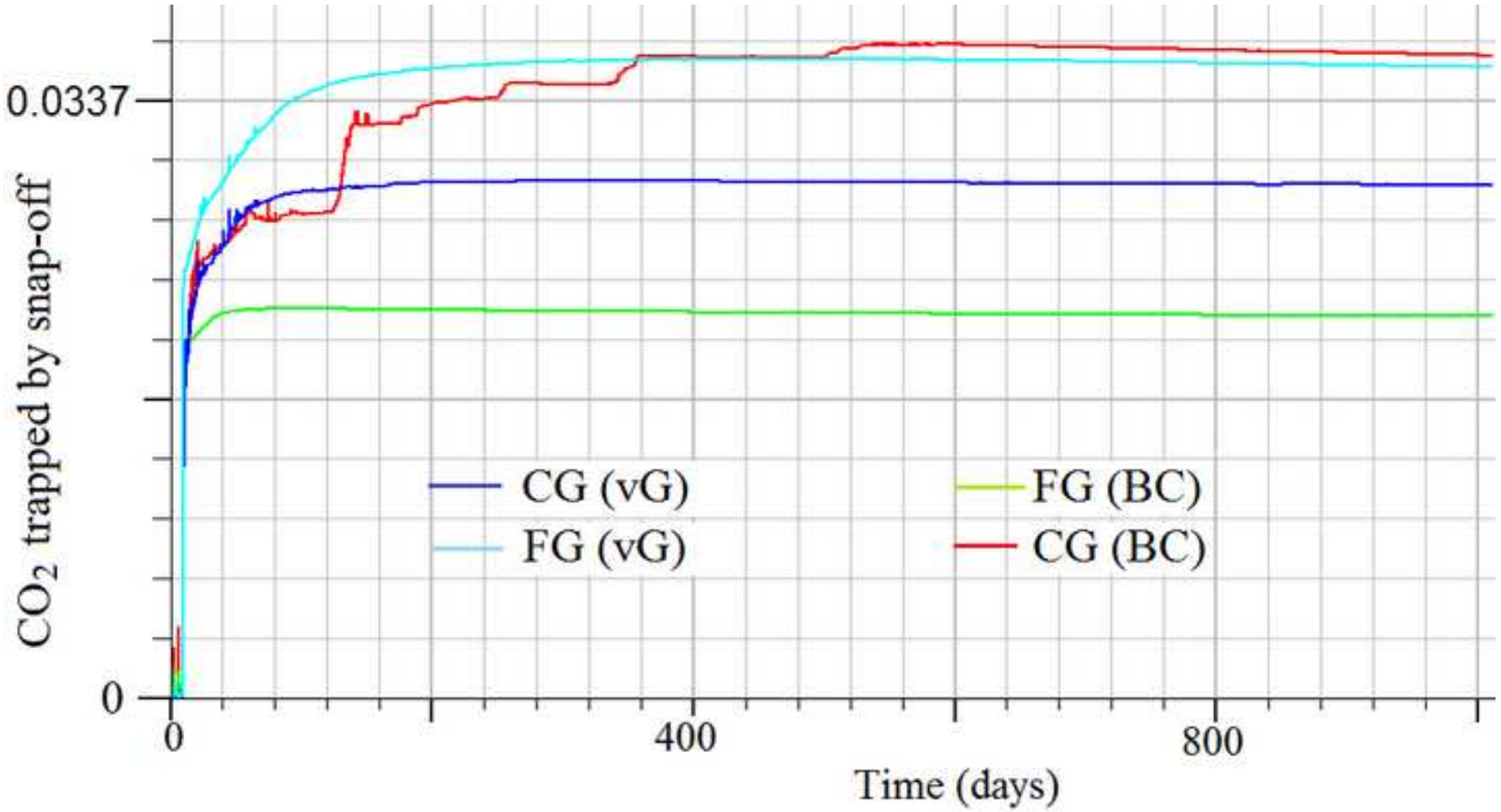
0.0337
0
CO_2 trapped by snap-off
CG (vG)
FG (vG)
FG (BC)
CG (BC)
0
400
800
Time (days)

Figure 13

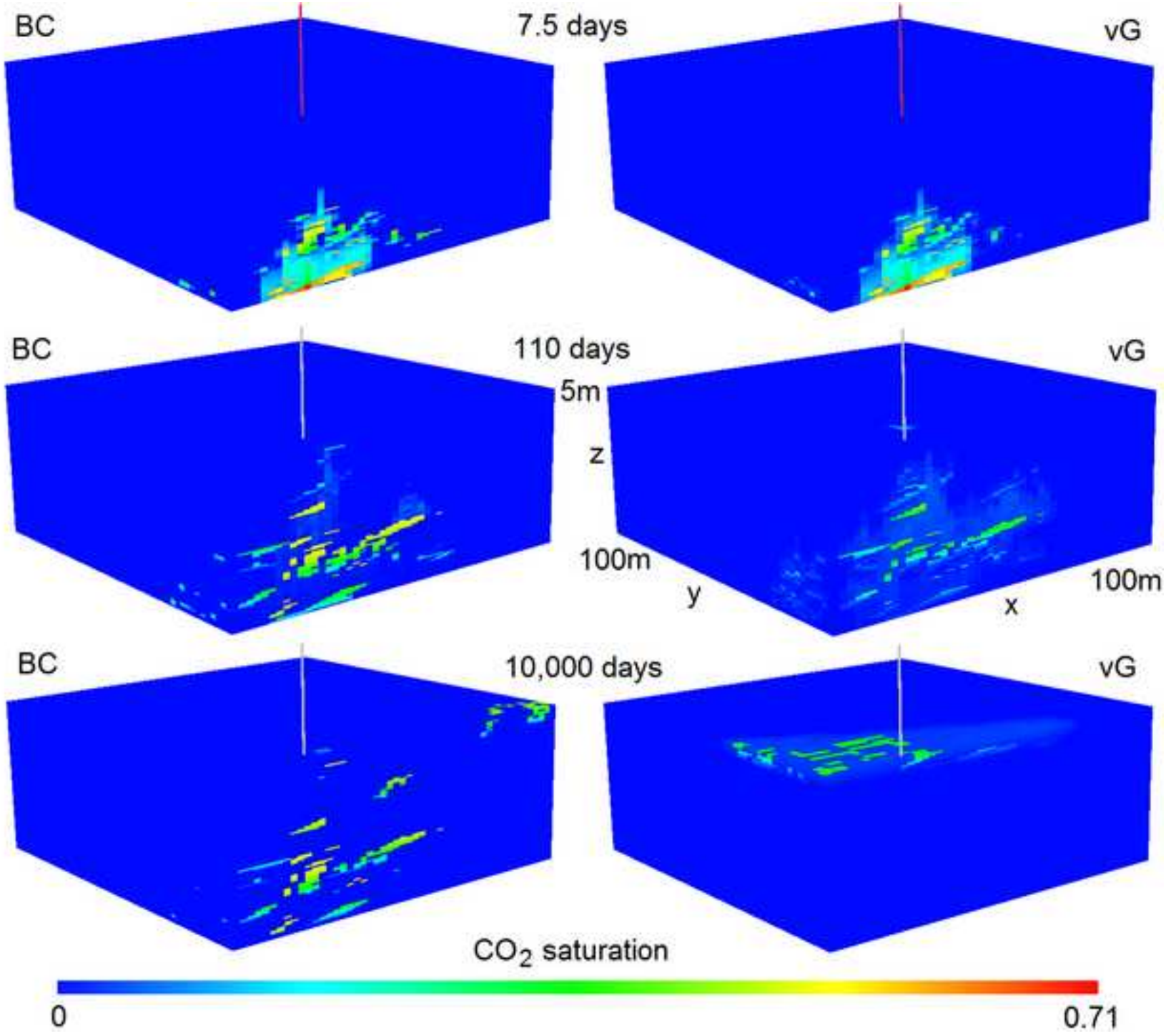
BC
7.5 days
vG
BC
110 days
vG
5m
z
100m
y
x
100m
BC
10,000 days
vG
CO2 saturation
0
0.71